The influence of subaquatic springs in lacustrine sedimentation: origin and paleoenvironmental significance of homogenites in karstic Lake Banyoles (NE Spain)

Mario Morellón*[1, 2], Flavio S. Anselmetti[3, 2], Blas Valero-Garcés[4], Santiago Giralt[5], Daniel Ariztegui[6], Alberto Sáez[7], M. Pilar Mata[8], Fernando Barreiro-Lostres[4], Mayte Rico[4], Ana Moreno[4]

[1] *Instituto de Geociencias (CSIC, UCM),Calle José Antonio Nováis, 2, 3ª planta, 3b. Facultad de Ciencias Geológicas, Univ. Complutense. 28040 Madrid, Spain.*

[2] *Swiss Federal Institute of Aquatic Science and Technology, Eawag, Ueberlandstrasse 133, CH-8600 Dübendorf, Switzerland.*

[3] *Institute of Geological Sciences and Oeschger Centre of Climate Change Research, University of Bern. Baltzerstrasse 1. CH-3012 Bern, Switzerland.*

[4] *Department of Environmental Processes and Global Change. Pyrenean Institute of Ecology (IPE) – CSIC. Campus de Aula Dei. Avda Montañana 1005. E-50059 Zaragoza, Spain.*

[5] *Institute of Earth Sciences Jaume Almera (ICTJA-CSIC). Carrer Lluis Sole i Sabaris s/n. E-08028 Barcelona, Spain.*

[6] *Section of Earth Sciences. University of Geneva. Rue des Maraîchers 13. CH-1205 Genève, Switzerland.*

[7] *Department of Stratigraphy, Paleontology and Marine Geosciences. Universitat de Barcelona. C/ Marti Franques s/n. E-08028 Barcelona, Spain.*

[8] *Instituto Geológico y Minero de España (IGME). C/ Calera 1. E-28760 Tres Cantos (Madrid), Spain.*

*Corresponding author. E-mail address: mario.morellon@igeo.ucm-csic.es

ABSTRACT

Banyoles (42º08'N, 2º45'E) is the largest and deepest lake of karstic-tectonic origin in the Iberian Peninsula. The lake comprises two basins and six sub-circularly shaped sub-basins fed by subaqueous springs. Periods of intense groundwater inflow in the deepest sub-basins lead to the fluidization and re-suspension of previously deposited sediments and subsequent settling forming homogenite deposits on the southern basin intermediate platforms. The multiproxy analysis of sediment cores combined with high resolution seismic stratigraphy (3.5 KHz pinger and multi-frequency Chirp surveys), allows a precise reconstruction of depositional environments and related hydrological variability and groundwater inflow during the last ca. 7.6 cal kyrs BP. According to the age model based on $^{137}Cs/^{210}Pb$ and AMS ^{14}C dating, homogenite deposition occurred between 7.2 and 5.5 cal kyrs BP, stopped during the middle Holocene (5.5 - 2.8 cal kyrs BP) and greatly increased during the last two millennia with a total of 17 homogenite layers up to 75 cm-thick. The onset of this unique sedimentation mode ca. 3 cal kyrs BP coincides with an increase in lake level, evidenced by the onlapping of fine-grained, distal sediments over coarser massive, carbonate-rich, littoral deposits. A detailed, multidisciplinary study of the homogenites (sedimentology, physical properties, high-resolution elemental geochemistry, mineral composition, grain-size, organic matter content and SEM) combined with seismic stratigraphy demonstrates that the fluidization events triggering the formation of the homogenites were caused by higher and more intense local groundwater inflow, related to increased rainfall during the Late Holocene and likely intensified by land use changes during the last millennia.

Keywords: karstic lake, subaquatic springs, groundwater, turbidity plumes, homogenites, Holocene

1. Introduction

Groundwater constitutes an essential hydrological resource in Mediterranean areas characterized by a summer drought period and frequent negative hydrological balance phases, which are particularly threatened by global change (García-Ruiz et al., 2011; Younger et al., 2002). In these regions, aquifers are essential for sustaining human activities and limnic ecosystems, (Álvarez-Cobelas et al., 2005; Edmunds et al., 2004; Shapley et al., 2005). The groundwater input to the hydrological balance is rarely quantified in most lakes, however, subaqueous springs are commonly identified as a significant source for groundwater in lake systems (Assayag et al., 2008; Canals et al., 1990; Colomer et al., 2002; Matter et al., 2010). Recently, such springs and associated pockmarks have been described and imaged thanks to high-resolution geophysical and limnological surveys (e.g., Lake Ohrid, (Matter et al., 2010), Lake Kivu (Ross et al., in review)). In spite of their variable relative importance in the hydrological balance of these systems, subaquatic springs commonly supply cool and oxygenated waters, rich in ions and nutrients, leading to the establishment of particular subenvironments and specific habitats for endemic species within lake systems (Descy et al., 2012a; Matter et al., 2010).

Ecological and limnological responses to subaquatic springs are well-studied (e.g., Dead Sea (Ionescu et al., 2012), Lake Bogoria (Dadheech et al., 2013), Lake Kivu (Descy et al., 2012b)) and extensive research has been carried out on associated carbonate sedimentary features (i.e., microbialites, tepee structures, diagenetic iron-rich shoreline indicators and carbonate crusts) (Burne and Moore, 1987; Rosen et al., 2004; Rosen et al., 2002; Warren, 1982; Winter, 1999). However, less attention has been paid to the physical effects of groundwater input in sedimentation and its potential to remobilize significant amounts of sediments (Bloesch, 1995; Draganits and Janda, 2003). Examples of fluidization and resuspension of offshore lake sediments and consequent re-deposition of thick ‘homogeneous’

layers have been exclusively described as a result of shaking and/or sub-aqueous mass-wasting slope processes caused by earthquakes (Beck, 2009). However, intense and focused groundwater input through subaquatic springs could be also able to produce a similar effect in sedimentation, not yet described in detail in lake settings. Although these groundwater-fed lake basins often provide long, continuous sequences with high temporal resolutions, suitable for palaeohydrological and palaeoclimate reconstructions (Morellón et al., 2009; Valero-Garcés et al., 2013), an adequate understanding of sedimentary processes is essential to reconstruct the evolution of groundwater inputs, their impact in lake sedimentation and their role in homogenite formation (Shapley et al., 2005).

Lake Banyoles (NE Spain) belongs to a groundwater-fed karstic system and constitutes a unique example in the Iberian Peninsula of offshore sedimentation partly controlled by the activity of sub-aqueous springs. Geophysical and limnological surveys during the last decades have documented the resuspension and fluidization of sediments by focused groundwater inflow at the deepest sub-basins of the lake (Canals et al., 1990; Casamitjana and Roget, 1993), leading to the development of turbidity plumes (Serra et al., 2005). These 'fluidization events' have been related with episodes of intense rainfall in the recharge area of the aquifer feeding the lake (Soler et al., 2009; Soler et al., 2007). Although Banyoles has been extensively investigated from a limnological point of view, the impact of groundwater dynamics on the sediments across the lake, and the spatial and temporal extent of this impact at longer timescales than the last few decades, remains unknown. Moreover, the depositional history of the lake has been exclusively studied at the littoral areas of the sedimentary basin (Cho Martínez, 2012; Höbig et al., 2012; Pérez-Obiol and Julià, 1994; Valero-Garcés et al., 1998) and at emerged pre-Holocene paleolake deposits (Julià-Brugués, 1977; Leroy, 1997; Løvlie and Leroy, 1995).

This paper aims to fill this gap in the investigations carried out in Banyoles and provides a Holocene sedimentary reconstruction using offshore sediments with special emphasis on sedimentary processes associated with fluidization events related to higher groundwater input episodes through subaquatic springs. The combined use of high-resolution seismic stratigraphy and a multi-proxy analysis of sediment cores recovered at offshore areas of the lake enable a precise reconstruction of the spatial extent, timing and different intensity of groundwater discharge. The associated sedimentary processes are evaluated in relation to climate variability and changes in land use during the last millennia.

2. Regional setting

2.1 Geological and geomorphological setting

Lake Banyoles (42º1'N; 2º4'E, 173 m a.s.l.), located in the NE margin of the Iberian Peninsula, 20 km west of the Mediterranean Sea (Fig. 1A) lies in a tectonic-karstic basin (Julià, 1980) and is formed by several cone-like karstic depressions (Fig. 1B). The lake is located in the eastern South-Pyrenean Foreland Basin (Bischoff et al., 1994; Burbank et al., 1992) affected by widespread Neogene extension (Saula et al., 1994; Tassone et al., 1994). The bedrock comprises the mid Eocene Banyoles Formation, mainly composed of marine, organic- and pyrite-rich marls and mudstones, underlain by the Eocene Beuda Formation consisting of massive gypsum (200-300 m), and the 100 to 200 m thick Perafita Formation dolostones (Barnolas, 1992; Mató i Palós et al., 1996; Serra-Kiel et al., 2003). The contact between these last two formations has led to a bedrock 'de-dolomitization' process due to gypsum dissolution, a particularly intense karstification mechanism responsible for the formation and collapse of the Lake Banyoles depressions (Bischoff et al., 1994). Karstic processes (e.g., collapse depressions, intermittent springs, karren fields) are still active in the lake catchment (Canals et al., 1990; Julià, 1980; Sanz, 1981), as demonstrated by the

12/11/1978 collapse, when a new sub-basin ('Estanyol Nou') was formed near to the southwestern shore (Höbig et al., 2012).

Lake Banyoles is the last remnant of a larger lacustrine basin developed during Pliocene-Quaternary times, known as the Banyoles-Besalú system, which occupied 90 km^2 (Canals et al., 1990; Julià-Brugués, 1977). Travertine formations and calcareous lithologies are common, both in ancient terraces (Julia Bruguès and Suc, 1980; Leroy, 1997) and present lacustrine deposits (Coma et al., 1988; Coma et al., 1987). The age of the travertine formation damming the eastern margin of the modern lake is ~120 to 45 ka BP (Julià and Bischoff, 1991), which represents the potential maximum age of the lacustrine deposits accumulated within the basin.

The littoral zone of the modern lake (0-3 m water depth) is covered by a thin macrophyte vegetation belt of *Phragmites, Schoenoplectus* and *Myriophyllum*. Sediments range from travertines and calcareous sands in the littoral areas, to carbonate-rich silts and clays in the distal areas (Rieradevall and Roca, 1995).

2.2 Morphometry, hydrology and limnology of the lake

The lake has a N-S elongated shape and a surface of 118 Ha. The lake is formed by 7 main circular-shaped sub-basins (B1 to B6), with steep margins and water depths ranging from 7.5 to 44 m, connected by shallower, flat platforms (ca. 20 m and 5-10 m water depths in the southern and northern areas, respectively) (Canals et al., 1990; Moreno-Amich and García-Berthou, 1989) (Fig. 1B). Karstic depressions confer a lobed shape to the lake shoreline, and a shallow (< 12 m maximum water depth) and narrow (< 500 m) sill in the center divides the lake in two basins, here referred as northern and southern ones (Fig. 1B).

The lake is hydrologically open and mainly groundwater-fed through subaqueous springs located in the deepest sub-basins of the southern basin (B1 and B2) (Canals et al.,

1990; Moreno-Amich and García-Berthou, 1989). Surface water input derived from the 11.42 km^2 catchment drained by the creeks located in the western area of the lake has been quantified as 100 to 300 l/s for May-September 1984, whereas output through the canals at the eastern margin (Fig. 1C) ranges from 568 to 1080 l/s for the same period (Canals et al., 1990; Dutras et al., 1986). Thus, groundwater supplies 85% of the total water input (Casamitjana et al., 2006). Lake water in southern basin is characterized by a lower residence time and higher oxygenation levels than water in the northern lobe. Particularly, sub-basin B1 provides 90% of groundwater input (Serra et al., 2005). The other main sub-basins of the northern basin (Fig. 1B) have a lower groundwater input so that anoxic conditions and sulfide production at the hypolimnion occur (Garcia-Gil et al., 1993; Guerrero et al., 1978). Thus, the 6 sub-basins are connected by their epilimnetic waters, but their respective hypolimnions are isolated and show differential anoxic periods, ranging from 1 to 12 months/year (Prat and Rieradevall, 1995).

Surface lake waters are sulphate and calcium-rich ($[SO_4^{2-}] > [HCO_3^{2-}] > [Ca^{2+}] > [Mg^{2+}]$) (Bischoff et al., 1994), with an electrical conductivity of 1300 to 1400 µs/cm and a pH between 7 and 8.1 (MAGRAMA, 2006). Water temperature is highly variable, ranging from 8 to 25 °C depending on the water depth and season (Rieradevall and Roca, 1995). Oxygenation conditions are also spatially variable and depending of groundwater input, ranging from oxic (0-7 m water depth), to one month of anoxia (sub-basin B1>12 m water depth), and to long-lasting anoxia (sub-basins B3 and B4, >12 m) (Rieradevall and Roca, 1995). The lake is monomictic, with water stratification from April to October. A chemocline is also present in sub-basins B1 and B4 at 19-20 and 13-17 m water depth respectively, which leads to long anoxic periods in the hypolimnion (Rieradevall and Roca, 1995).

Differences in the thermal inertia and incoming flux through the subaqueuous springs, located in the northern and southern basins, move denser water during the winter season from

177 the shallower northern to the deeper southern basin. This leads to a bottom current with a flow
178 of 20000 l/s and a velocity of up 12 cm/s that redistributes water between the two basins,
179 replacing northern basin waters every ~5 days. This exchange constitutes the main current
180 dominating circulation in the lake (Casamitjana et al., 2006; Roget et al., 1993).
181
182 *2.3 Groundwater and turbidity plumes*
183 The lake constitutes a 'trop-plein' of a complex aquifer system whose recharge area is
184 located in the Alta Garrotxa Range, 15 to 40 km northwards (Brusi et al., 1990; Sanz, 1981).
185 The NE-SW trending Albanyà fault, east of the lake, constitutes a subvertical dam for the
186 groundwater (Moreno-Amich and García-Berthou, 1989). Most of the deepest sub-basins (B1,
187 B2, B4, B5 and B6) are filled with several meters of sediments maintained in suspension by
188 the intense groundwater inflows forming a sharp and horizontal, upper sediment interface,
189 known as the lutocline which is recognizable in seismic profiles (Fig. 1D) (Canals et al.,
190 1990). These suspensions have particle concentrations varying from 0.18 to $< 10^{-3}$ g/l and
191 rather constant temperatures (~19ºC) (Casamitjana et al., 2006). According to geophysical
192 surveys and sedimentological analyses, sediments in B1, B3 and B4 appear as 'mobile'
193 particles in suspension, whereas they are usually denser and more consolidated in B2,
194 resulting in an acoustic bedding at the bottom of this sub-basin (Colomer et al., 2002). The
195 momentum of the underground spring and sediment grain-size determines the maximum
196 height that the lutocline can rise to in each case (Casamitjana et al., 1996; Colomer et al.,
197 1998). Fluctuations of the lutocline depths in B1, B3 and B4 are comparatively smaller than
198 B2 and show consistent shifts (Casamitjana and Roget, 1993).
199 Most intense fluidization and re-suspension processes, and associated hydrothermal
200 plumes, are restricted to the deepest sub-basins B1 and B2. Sub-basin B1 is fed by the largest
201 groundwater flow (~500 l/s). Its sediment fill has a vertical thickness of 45 to 50 m and a

sediment density of 100 to 130 g/l (Colomer et al., 2002). Its lutocline oscillates from 29.2 to 32.0 m water depth (Serra et al., 2005) (Fig. 1D). In contrast, B2 experiences periodical large fluctuations in sediment density from 280 to 180 g/l and larger lutocline migrations (from 25 to 45 m). Sediment fluidization processes occurs episodically associated with particular intense rainfall events in the aquifer recharge area (average monthly values 1.5 to 4.5 times larger than the long term mean (1970-1999) (Colomer et al., 2002). Thus, sub-basin B2 acts as an overflow of the groundwater system.

Due to the difference between temperature of the lutocline and the hypolimnetic water immediately above B1, an upward-directed permanent hydrothermal plume develops (Colomer et al., 2001). This plume carries a suspension of particles from the lutocline up to a maximum height, which varies depending on the stratification depth of the water column. During the mixing period, this plume reaches the surface of the lake, spreading laterally and forming a ~7 m-thick turbidity current, with a sediment concentration of ~0.01 g/l (Serra et al., 2005). According to sediment-trap studies, particle fluxes oscillate from 10 to 25 g m^{-2} day^{-1} near to B1 to < 5 g m^{-2} day^{-1} in more distant areas of the southern basin (Serra et al., 2002; Serra et al., 2005).

An additional temporal, hydrothermal turbidity plume develops above sub-basin B2 due to fluidization events after intense rainfall in the aquifer recharge area (Soler et al., 2009). The onset of the fluidization is characterized by episodic ground-water influx entering through preferential paths in the more consolidated sediment at the bottom of sub-basin B2. The water pressure through small diameter conducts within the sediment causes a high mean upward velocity, which is three orders of magnitude greater than in perennial plume B1. After such an event, water-flux velocity decreases progressively and resuspends the settled sediment. Finally, when sediments are totally fluidized, the episodic hydrothermal plume of sub-basin B2 resembles that of the perennial plume of B1 (Soler et al., 2009). When the

hydrothermal plume in sub-basin B2 is fully developed, a large quantity of sediment is transported upwards from the lutocline, resulting in an increase in sedimentation rates in the southern basin (ca. 156 g m^{-2} day^{-1}), which is one order of magnitude higher than in periods without fluidization, when only the B1 hydrothermal plume remains active (Casamitjana et al., 2006; Serra et al., 2002; Soler et al., 2009).

As both basins of the lake (N and S) are separated by a shallow sill (Fig. 1B), sediments transported by turbidity plumes are restricted during the stratification period to the southern one. In contrast, during the mixing period, particles can reach the surface of the lake, spreading laterally and subsequently settling across the entire lake bottom (Soler et al., 2009). However, sedimentation in the northern basin is not significantly affected by re-suspended sediments and carbonate-rich silts and sands with abundant encrusted charophyte stems and other calcitic bioclasts (e.g., ostracods, gastropods) are predominant (Serra et al., 2005). Thus, the effect of turbidity plumes on sedimentation is mostly restricted to the southern basin.

3. Materials and methods

A geophysical survey was carried out in April 2011 using a high-resolution, single-channel seismic system with a centre frequency of 3.5 kHz (GeoAcoustic pinger source) and a EdgeTech Chirp 3100-P multi-frequency profiler, covering 22 km and 14 km of seismic lines, respectively. This dense grid consisting of ~36 km of seismic lines provides a mean spatial resolution of ~100 m between each line (Fig. 1C). Seismic processing workshop software was used for the processing of the pinger data (bandpass filter, flat gain) and the resulting seismic data set was interpreted using the Kingdom Suite software.

In May 2011, three pairs of overlapping sediment cores (BAN-11-1A, 2A and 3A) with maximum lengths of ~13, 12 and 5 m, respectively, were recovered using an Uwitec© percussion coring equipment installed on a floating raft. This research focuses on core 1A,

252 recovered in the flat platform between sub-basins B1 and B2, at ca. 21 m water depth.
253 Additional coring sites 2A and 3A are located in the northernmost area of the lake and sub-
254 basin B3, respectively. Three short, gravity cores were obtained to recover the uppermost part
255 and the sediment/water interface of the three sequences. Seven additional short cores (BAN-
256 12-1, 2, 3, 4, 5, 6 and 8) were recovered in July 2012 along a transect between B1, B2 and the
257 location of the longest core BAN-11-1A (Fig. 1C). Cores recovering suspended sediments of
258 sub-basins B1 and B2 (BAN-12-1 and 2) were maintained in upright position until sediments
259 were stable and settled down, before excess water was eliminated. The uppermost 60 cm of
260 the BAN-11-1A sequence was sub-sampled in the field every 1 cm for ^{137}Cs and ^{210}Pb dating.
261 Physical properties (magnetic susceptibility, gamma density, P-wave velocity) were
262 measured in core BAN-11-1A with a Geotek Multi-Sensor Core Logger (MSCL) every 1 cm.
263 All the cores were subsequently split in two halves and imaged with a digital camera. The
264 Lightness (L*) parameter was obtained from the core pictures using Adobe Photoshop CS and
265 Image J software. Lithotypes were defined after visual and microscopic smear slides
266 observation, applying the methodology described in (Schnurrenberger et al., 2003) (Table 1).
267 Elemental composition of core BAN-11-1A sediments was obtained by using an
268 AVAATECH XRF core scanner at a resolution of 5 mm and under two different working
269 conditions: i) with an X-ray current of 0.8 mA, at 10 s count time and 10 kV X-ray voltage for
270 the measurement of Al, Si, P, S, Cl, Ar, K, Ca, Ti, V, Cr, Mn and Fe; and ii) with an X-ray
271 current of 2 mA, at 30 s count time and 30 kV X-ray voltage for the measurement of Ni, Cu,
272 Zn, Ga, Ge, As, Se, Br, Rb, Sr, Y, Zr, Nb, Au, Pb, Th and U. The XRF results are expressed
273 as counts per second (cps) and only chemical elements with mean cps over 1500 were
274 considered to be statistically significant.
275 Grain size of short cores BAN-12-1 and 2 was measured every 4 cm. Core BAN-11-
276 1A was measured at variable resolutions: for grain size: ~8 cm at the uppermost 610 cm and

277 ~25 cm at the lowermost part of the sequence, for TOC and TIC every 3 cm, and for X-ray
278 diffraction every 9 cm. Grain size was determined using a Malvern Mastersizer 2000.
279 Samples were pre-treated with 15% hydrogen peroxide in a hot plate at 80°C to eliminate the
280 organic matter; a dispersant agent and ultrasound treatment were used prior to measurement.
281 Total organic carbon (TOC) and total inorganic carbon (TIC) were measured with a LECO
282 SC 144 DR elemental analyzer. Whole sediment mineralogy was characterized by X-ray
283 diffraction with a Bruker-AXS D5005 (working conditions: Cu kα, 40 kV, 30 mA and
284 graphite monochromator) and relative mineral abundance was determined using peak
285 intensity following the procedures described in (Chung, 1974a; Chung, 1974b). Results are
286 expressed in percentages with respect of the total dry weight of the sample.

287 Scanning electron microscope images were taken at dried sediment samples of cores
288 BAN-11-1A, BAN-12-1 and -2 under low-vacuum conditions in an environmental scanning
289 electron microscope FEI Inspect on uncoated fragmented samples. Backscattered electron
290 (BSE) images were obtained in order to detect compositional differences of the components
291 as grey level contrast. In addition, energy dispersive X-ray spectrometry (EDS) analysis was
292 performed when necessary.

293 The chronology of the lake sequence is based on: i) 9 Accelerator Mass Spectrometry
294 (AMS) ^{14}C dates from core BAN-11-1A, analyzed at the ETH-Zürich Laboratory of Ion Beam
295 Physics and at DirectAMS radiocarbon services (Seattle, USA) (Table 2) and on ii)
296 $^{137}Cs/^{210}Pb$ dating by gamma spectroscopy at Eawag (Dübendorf, Switzerland). Excess
297 (unsupported) ^{210}Pb was calculated as difference between total ^{210}Pb and ^{226}Ra for individual
298 samples. Corrected radiocarbon dates were converted into calendar years BP with Calib 6.0
299 software using the INTCAL 09 calibration curve (Reimer et al., 2009), selecting the median
300 of the 95.4% distribution (2σ probability interval) (Table 2). The age-depth relationship was

301 constructed by linear interpolation of the 1963 AD ^{137}Cs maximum activity peak and
302 calibrated radiocarbon dates using Analyseries (Paillard et al., 1996).
303
304 **4. Results**
305 *4.1 Seismic Stratigraphy*
306 In spite of frequent gas masking throughout the lake basin, locally high penetration
307 into the sub-surface down to the acoustic basement allowed tracking of the bedrock
308 morphology in many parts of the lake. Maximum seismic penetration up to 20 m in the
309 northern basin of the lake (Fig. 1D), where gas masking is more frequent, and 18 m in the
310 southern basin (Fig. 2) did not reach the substratum. These two basins -separated by a shallow
311 sill with no seismic penetration (Fig. 1D)- show a different seismic stratigraphy due to their
312 complex bathymetry and variable sedimentological processes. The southern basin is
313 characterized by the flat bottom areas in B1 and B2 (Fig. 1B and D), corresponding to the
314 lutoclines (Canals et al., 1990), and extensive and rather flat areas at ~20 m water depth
315 between and around these two main depressions, displaying moderate seismic penetration
316 (Fig. 2). The bedrock surface was identified in a previous lower-frequency survey (150-2000
317 kHz) (Canals et al., 1990) and is characterized by local irregularities and discrete steps and
318 sharp edges, consistent with the karstic origin and active dynamics of the two depressions.
319 Seismic stratigraphic analysis of our 3.5 kHz survey allowed the identification of three
320 major seismic units (SA-SC; Figs. 2) and several seismic horizons, which have been tracked
321 through the southern basin. These horizons and units were correlated with the core
322 lithostratigraphy (see below). A constant acoustic velocity of 1500 m/sec based on the MSCL
323 measurements has been used for the seismic-to-core correlation (Fig. 2A).
324 The oldest seismic unit (*Unit SA*) reaches more than 10 m thickness and is only
325 recognizable in areas located close to the E lake margin. It is characterized by rather

326 continuous, mid-amplitude reflections and intercalated seismically more transparent units up
327 to 2 m thick. The lowermost part of core BAN-11-1A reached the uppermost part of this
328 seismic unit (Fig. 2A).

329 *Unit SB* is visible only in few areas and consists of continuous low-amplitude
330 reflections with the intercalation of two higher amplitude reflections, coinciding with rather
331 homogeneous lithology (Fig. 2A).

332 The youngest seismic unit *(Unit SC)* has been mapped through larger areas of the
333 southern basin and reaches ~10 m in thickness in the central areas of the platforms. Seismic
334 facies are characterized by the alternation of high-amplitude, laterally continuous reflections
335 and transparent layers, slightly increasing basinward in thickness up to ~1 m thick (Fig. 2).
336 The upper part of this seismic unit onlaps over SA and SB units and corresponds in sediment
337 core 1A with a lithological change to sediments with higher and more variable density (Fig.
338 2A).

339

340 *4.2 Sedimentology*

341 *4.2.1 Lithotypes*

342 Six lithotypes have been defined in the long (BAN-11-1A) and short (BAN-12-1 to 8)
343 sediment cores recovered from the southern areas of Lake Banyoles, on the basis of detailed
344 sedimentological descriptions, smear-slide and SEM microscopic observations and
345 compositional analyses. According to textural and compositional criteria, these lithotypes
346 have been grouped into two main categories: i) banded to laminated and ii) massive (Table 1,
347 Figs. 2, 3 and 4).

348 Banded and laminated lithotypes (Fig. 4A, B and C) are composed of variable
349 amounts of: i) mud-size (10-15 μm) elongated Low Magnesium Calcite (LMC) crystals
350 derived from direct precipitation from lake waters (Fig. 5B), ii) reworked biogenic particles

from the littoral areas (*Chara* fragments, micrite oncoids, ostracods and gastropod fragments of different sizes (<50 µm)); iii) diatoms and other organic components (Figs 5A, C.); and iv) detrital particles, including carbonates, quartz grains and clay minerals (mainly illite and chlorite) derived from the weathering and erosion of the soils and bedrock in the watershed (Figs. 3 and 5A). Grain-size distribution is dominated by the silt fraction, with mean values ranging from 5 (lithotype 1) to ~20 µm (lithotype 3) (Table 1, Fig. 3).

Massive lithotypes (Fig. 4D, E and F) occur as:

i) up to 120 cm thick, fining upwards sequences, ranging from carbonate-rich sands (lithotypes 6, ~65 µm mean grain size) to fine-grained silts capped by clay-sized particles at the top (lithotype 5, ~10 µm mean grain size). These sediments are more carbonate-rich than banded and laminated lithotypes (Fig. 3) and contain higher amounts of coarse and fine-grained particles (from sands to silts) of reworked components (fragmented bioclasts, sub-rounded grains) (Fig. 5D, E and F). They are restricted to the lowermost part of the recovered succession and deposited by turbidity currents caused by the collapse of littoral areas (mass-wasting deposits) (Figs. 3 and 4F)

ii) 'homogenites' (lithotype 4) occurring as 2 to ~75 cm-thick layers lacking any clear vertical grain-size distribution, composed of poorly sorted, fine-grained silts with mean sizes ranging from 6 to 12 µm (Figs. 3 and 4E). These layers are likely deposited after the fluidization of sediment particles maintained in suspension at the deepest sub-basins of the lake (B1 and B2) and they are more abundant in the upper part of the sequence. They are described in detail below.

4.2.2 Cores stratigraphy

374 According to their lithology (Table 1, Fig. 3), the sedimentary succession in the
375 southern basin of Lake Banyoles has been divided into three main lithological units (LA, LB,
376 LC) matching with facies associations.

377 *Unit LA* (1298 to 970 cm core depth,) is characterized by the presence of carbonate-
378 rich, silty lithotype 3 at the base (Figs. 3 and 4C), leading to an alternation between more,
379 fine-grained lithotype 1 and relatively thin beds of massive lithotype 4 at in the middle of this
380 unit. A thick mass-wasting deposit (~120 cm), with a sandy layer at the base (lithotype 6) and
381 massive lithotype 5 occurs in the uppermost part of this interval (Figs. 3 and 4F). This unit
382 represents the transition from a relatively shallow, carbonate producing depositional
383 environment with bioturbation and thus, oxic conditions (lithotype 3) to a relatively deeper
384 setting (lithotype 1) accompanied by intensification of groundwater inflow (lithotype 4) and
385 mass-wasting activity (lithotype 6).

386 *Unit LB* (972 to 610 cm core depth) is characterized by the deposition of carbonate-
387 rich, silty lithotype 3 (Figs. 3 and 4C, Table 1), interbedding mm-thick layers of massive silts.
388 This unit deposited in a shallow, carbonate producing, oxic depositional environments with
389 abundant littoral fauna and variable detrital input.

390 *Unit LC* (610 to 0 cm core depth) starts with the deposition of banded to laminated
391 lithotype 2, reflecting more oxygen-depleted conditions associated with more distal/offshore
392 deeper depositional environments than Unit LB (Figs. 3 and 4B, Table 1). Upcore, sediments
393 are composed by an alternation of cm-thick fine-grained sediments interval (lithotype 1) and
394 thick layers of homogenites (lithotype 4) (Figs. 4D, E). This unit represents dominant distal
395 deposition at the coring site away from the slope of the margin of the lake, with relatively low
396 oxygenation conditions. The succession of lithotypes 3, 2 and 1 suggests a progressive
397 increase in lake level, confirmed by the seismic onlapping of unit C onto B (Fig. 2). The
398 deposition of up to 17 homogenite layers, with a maximum thickness of ~75 cm, also reflects

399 an abrupt intensification of groundwater activity during unit LC. The decrease in frequency
400 and thickness of lithotype 4 layers in the uppermost part of the succession is interpreted as a
401 decrease in groundwater activity in more recent times, accompanied by increased carbonate
402 and organic content (Figs. 3 and 6A).
403
404 *4. 3 Seismic to core correlation and depositional evolution*
405 Seismic to core correlation enables a basin-wide reconstruction of the main stages in
406 the Holocene depositional history of Lake Banyoles (**Fig. 2A)**.
407 On the basis of seismic facies and the alternation of density contrasts, seismic Unit SA
408 is interpreted as a sedimentary succession characterized by the intercalation of massive
409 lithotypes (4, 5 and 6) within a sequence from distal-fine grained lithotype 1 to littoral
410 carbonate-rich lithotype 3 (Figs. 2A and 3). Deposition of mass-wasting deposits and
411 turbidites – as the one > 1 m thick turbidite (lithotypes 5 and 6) at the top of this unit - could
412 have been more frequent during an early stage of development of the southern basin
413 depressions with more active karstic collapses. Additionally, several relatively thin (up to 25
414 cm-thick) homogenites (lithotypes 4 and 5) also occur at the lowermost part of this unit (Fig.
415 2A and 3).
416 According to lithology, low-amplitude reflections with the intercalation of two higher
417 amplitude reflections in SB are interpreted as the dominance of acoustically homogeneous,
418 carbonate-rich lithotype 3 deposits with frequent clastic intercalations. A basinward increase
419 in thickness (from ~4 m in coring location to more than 6 m in more distal areas) might be
420 related to the occurrence of mass-wasting deposits at the lower part of the recovered sequence
421 (Fig. 2).
422 Finally, seismic facies observed in uppermost unit SC correspond to the alternation
423 between lithotype 1 and thick homogeneous lithotype 4 layers, characterized by higher and

424 constant density values (Fig. 2A). The onlapping of this unit above lowermost ones (A, B)
425 suggest an increase of lake level associated with the deposition of more fine and distal
426 lithotypes 1 and 4; higher groundwater flow (main water source of Lake Banyoles) is likely
427 associated with these periods of higher lake level. Good lateral continuity of reflections and
428 thickening of seismically transparent units towards the deepest sub-basin B2 suggests that the
429 origin of homogeneous lithotype 4 is related to depositional processes around this sub-basin
430 (Fig. 2).
431
432 *4.4 Age model*
433 To construct the age model, a total of 9 radiocarbon dates from core BAN-11-1A
434 (Table 2) were used. Most of the dated samples correspond to bulk organic matter due to the
435 absence of terrestrial organic macro remains. A large reservoir effect is suspected as recent
436 sediments (44.5 cm depth) yielded an uncorrected age of 5460 ± 35 ^{14}C yr BP. To determine
437 this reservoir effect and their likely variability through time, we used two dual dates, each of
438 them from the same stratigraphic levels: i) at the top of the sequence, characterized by
439 sedimentation under relatively deep conditions, similar to present-day (lithotypes 1 and 4),
440 comparing ^{137}Cs maximum activity peak of 1963 AD and a radiocarbon date on bulk organic
441 matter (reservoir effect = ~5470 yrs); and ii) at the base of the core, with predominantly
442 shallow-water conditions (lithotypes 1, 2 and 4.2), comparing two radiocarbon dates derived
443 from a terrestrial macro-remain and bulk organic matter (reservoir effect = ~3025 years)
444 (Table 2).
445 The estimated reservoir effects for the top and the base of the core were subtracted
446 from radiocarbon dates made on bulk organic matter at lithological units LC and LA-LB,
447 respectively. A consistent result was obtained in lowermost units A and B, with a rather
448 constant sedimentation rate of ~0.1 cm / year (Fig. 7A). The comparatively higher reservoir

449 effect obtained for the uppermost unit C, characterized by higher lake levels, might be
450 explained by higher input of dissolved carbon from groundwater, likely higher during this
451 recent stage. Variations in groundwater flow and potential reworking of organic particles from
452 the deepest sub-basins B1 and B2 might also be responsible for the radiocarbon reversals
453 occurring within unit A. Thus, the three radiocarbon dates of units A and B were considered
454 for the chronology of the sequence, while all the other dates were rejected (Table 2, Fig. 7A).
455 Corrected dates were calibrated into calendar years and the age-depth relationship was
456 constructed by linear interpolation (Fig. 7A). Event layers, deposited instantaneously and
457 represented by massive lithotypes 4, 5 and 6 (i.e., homogenites in lithological units LA and
458 LC (Fig. 7A, B) and the mass-wasting deposit at the top of unit A), were subtracted from the
459 age model. According to this, the Lake Banyoles sequence spans the last ~7600 cal years BP.
460 The uppermost unit LC was deposited during the last ~2800 cal years. The age-depth
461 relationship shows an abrupt increase of sedimentation rate at the transition between units LB
462 and LC, from 0.1 cm / year to 0.23 cm / year, including event layers (Fig. 7A). The abundance
463 of these homogenites in the upper unit explains this sedimentary rate change (Fig. 7B). The
464 internal chronology for the uppermost unit, between the uppermost validated date (~2800 cal
465 yrs BP) and the 1963 AD maximum ^{137}Cs activity peak, remains unclear due to the lack of
466 dates. Three different models can be used as an approximation: model 1) an extrapolation of
467 ^{137}Cs inferred sedimentation rate throughout the interval containing the homogenites; model
468 2) an interpolation between ^{137}Cs peak and valid date (2800 cal yrs BP) at the uppermost part
469 of unit B; and model 3) an interpolation between ^{137}Cs peak and lowermost (not valid)
470 radiocarbon date of unit C. According to these different age models, the occurrence of
471 homogenites could be restricted to the periods 1840-1938 AD, 380-1600 AD and 1340-1720
472 AD, respectively (Fig. 7B).
473

4.5 Sedimentological and geochemical characterization of homogenites

Lithotype 4 is dominant throughout the uppermost part of the sequence (lithological unit LC) (Figs. 3 and 6A) and is also present occasionally at the lowermost unit LA, recovered in the platform between deepest sub-basins B1 and B2. These intervals are defined by their regular colour, texture and composition, with minor or no internal variations. Compared to intercalated lithotype 1, they are characterized by a lighter colour (higher L* values, > 60), higher magnetic susceptibility (MS), higher density and a slightly coarser grain size, as evidenced by higher mode (~6 μm) and mean values (6 to 12 μm) (Figs. 3, 4E and 6A).

These homogenites are also characterized by a slightly higher organic and carbonate content (as recorded by TIC, calcite and higher Ca and Sr values) (Figs. 3 and 6A). Consequently, they have a relatively lower concentration on siliciclastic minerals (quartz and clay minerals) and elements associated with this fraction (Al, Si, K, Ti, Zr, Fe, Mn) as summarized by lower Ti/Ca values (Fig. 6B). Other geochemical properties characterizing lithotype 4 are: i) a lower Sr/Ca ratio, likely revealing a lower proportion of aragonite, common in biogenic particles mostly reworked from littoral, carbonate-producing areas of the lake; ii) higher S values; and iii) a higher Fe/Mn ratio, likely indicating more local anoxic conditions during the deposition of these layers (Fig. 6A).

Detailed inspection of SEM images supports previous textural and compositional analyses (Fig. 3) and reveal: i) slightly coarser grain size in homogenites than facies 1 (Figs. 5A, D), ii) more evidences of transport and reworking in homogenites (broken diatoms, irregularly shaped grains, etc.) (Figs. 5D, E, F), iii) a higher content of well-developed, endogenic and regular calcite crystals in lithotype 1 (Fig. 5B), iv) a higher content of pyrite framboids in homogenites likely related to higher S concentrations (Fig. 5E) and v) the exclusive presence of the most fragile terrestrial components (e.g., plant remains) in offshore/distal deposits of

499 lithotype 1 (Fig. 5C). Moreover, reworked planktonic calcareous algae remains exclusively
500 occur in the homogenites of lithotype 4 (Fig. 5E).

501 Suspended sediments recovered below the lutoclines of the deepest sub-basins B1 and B2
502 show a very similar sedimentary features compared to homogenites, characterized by light
503 grey colours (slightly reddish in B1 and bluyish in B2) (Figs. 4G and H). Both homogenites
504 and sediments from these sub-basins are, when compared with offshore/distal lithotype 1,
505 characterized by higher carbonate content as reflected by higher Ca/Ti ratios (Fig. 6B).
506 Average mean grain sizes in B1 and B2 average 8.6 and 9.6 µm, respectively, slightly coarser
507 than in the homogenites (6.5 µm).

508

509 **5. Discussion**

510 *5.1 Homogenites and fluidization events*

511 Textural and compositional analyses of lithotype 4 deposits show a strong
512 homogeneity along the whole layer, particularly visible within uppermost unit LC (Figs. 3 and
513 6A). Good lateral correlation of these 'homogenites' between long and short cores (Fig. 8)
514 and inspection of seismic lines (Fig. 2) show that these deposits, absent in the northern basin
515 of Lake Banyoles, appear clearly 'thinning' towards the edges of the southern basin and
516 'ponding' offshore towards deepest sub-basins B1 and B2 (Fig. 2 and 8). These layers are
517 characterized by transparent seismic facies with no significant lateral changes (Fig. 2). The
518 origin of homogenites is usually attributed to allochthonous (i.e., distal part of a turbidite
519 initiated by a mass-wasting process in littoral areas turning into hyperpycnal (turbidity
520 currents with bed-load and suspended load)) or autochthonous sources (liquefaction,
521 resuspension) (Beck, 2009).

522 Turbidites are usually characterized by single, fining upwards sequences (Girardclos et
523 al., 2007; Hsü and Kelts, 1985; Schnellmann et al., 2005). However, in Banyoles, only the

524 homogeneous layer located at the top of lithological unit LA displays these particular
525 sedimentological features (Figs. 2A, 3 and 4F), and thus, is interpreted as a turbidite deposit
526 likely triggered by a mass-wasting episode. On the other hand, considering the location of
527 core BAN-11-1A, less than 100 m far from the lake shore, the presence of coarser grain
528 particles at the base of these deposits would be also expected if the area source was the littoral
529 of the lake, as described in other similar karstic lakes in the Iberian Peninsula (Morellón et al.,
530 2009; Valero- Garcés et al., 2013).

531 In contrast to turbidite deposition, formation of homogenites in upper unit C involves
532 liquefaction in the deeper sinkholes, resuspension of sediments and vertical transport and
533 settling of the particles in the platform areas. In fact, these mechanisms of transport and
534 deposition have been described for most of the deep sub-basins of the lake, with particular
535 intensity for sub-basins B1 and B2 as a result of intense groundwater inflow (Serra et al.,
536 2002; Soler et al., 2009). Fluidization and resuspension processes in lake sediments can also
537 result from shaking caused by earthquakes. However, this process should be rejected since
538 this region has a low to moderate seismic activity related to some Pyrenean Range faults and
539 only few earthquakes have been described (Secanell et al., 2004). The only relatively intense
540 (M_w = 6.5) earthquake recorded during historical times occurred in 1427 AD, with the
541 epicenter located ~22 km SW to the lake (Olivera et al., 2006) and likely caused shaking in
542 the lake basin. Nevertheless, given the low frequency of intense earthquakes and the high
543 frequency of homogenite events, seismic activity in the area cannot be considered as the
544 exclusive potential triggering mechanism for the deposition of this high number of
545 homogenites.

546 Comparison of homogenites with sediments accumulated at the deepest sub-basins (B1
547 and B2), corresponding to cores BAN-12-1 and 2, reflects many textural and compositional
548 similarities from the macroscopic scale, as observed in core images (Figs. 3, 4 and 6B) to the

549 microscopic level, as observed in SEM images. Although the range of variation in grain size
550 is relatively small in general, and within unit C in particular, homogenites are slightly coarser
551 (Fig. 3), with values closer to BAN-12-1 and 2, averaging 8.6 and 9.6 μm, respectively. From
552 the compositional point of view, Ti/Ca ratios of lithotype 4 and short cores BAN-12-1 and 2
553 are also similar and generally lower than lithotype 1 (Fig. 6B). Thus, a common sediment
554 source between B1 and B2 and homogenites is suggested. The marginal location of core
555 BAN-11-1A within the flat platform between B1 and B2 might explain this decreasing grain
556 size from B1 and B2 (8.6 μm and 9.6 μm), as coarsest particles transported by turbidity
557 plumes do not probably reach this area, as predicted by previous studies (Serra et al., 2002;
558 Serra et al., 2005).

559 According to recent limnological monitoring, there is a permanent contribution of
560 sediment particles derived from turbidity plume developed above B1 (Colomer et al., 2001;
561 Serra et al., 2005). Particle sediment fluxes in areas near coring site BAN-11-1A, close to the
562 shallow platform margins, between B1 and B2, do not reach 5 g m^{-2} day^{-1} (Serra et al., 2002;
563 Serra et al., 2005). Therefore, this plume might contribute to < 1 mm/year of sediment
564 thickness in this area and thus, is responsible for a relatively low important contribution of
565 particles, decreasing in size and number towards lake platform marginal areas, where coring
566 site BAN-11-1A is located (Fig. 8). Consequently, the relatively low sedimentation rate
567 produced by this plume is not able to accumulate the high thickness of homogenites sediment.
568 In fact, reddish, massive grained silts derived from B1 are spatially restricted to the edges of
569 this sub-basin and they do not normally reach more than 50 m far from the source area (Fig.
570 8). Furthermore, the frequent but episodic deposition of these homogenites must result from
571 an episodic and relatively rapid process rather than from a continuous, variable permanent
572 depositional mechanism.

573 In contrast, the second and stronger plume developed periodically above B2, as a result of
574 extraordinary intense groundwater inflow caused by intense rainfall in the recharge area of the
575 aquifer (Soler et al., 2009), has a particle sediment flux of 156 g m^2 day^{-1} (one order of
576 magnitude higher than B1), so that it is able to accumulate more than 1 cm of sediments per
577 year in the marginal areas of the platform located between B1 and B2. Taking into account
578 that homogenite thicknesses display a high range of variability (from 2 to 76 cm) and the
579 expected variability in the flow velocity for this turbidity plume, associated with the variable
580 diameter of karstic conducts within B2, this is the most likely depositional mechanism able to
581 produce homogenites.

582 In fact, correlation between short cores recovered between B1 and B2 and seismic line
583 (Fig. 8) document how most of the uppermost homogenites (reflected as transparent seismic
584 facies) are ponding predominantly towards sub-basin B2 and get thinner towards the edge of
585 the lake and B1. This depositional pattern suggests fluidization and resuspension of sediments
586 in sub-basin B2 as a result of particularly intense rainfall episodes in the recharge area of the
587 aquifer as the most likely mechanism for the deposition of homogenites in Lake Banyoles.

588

589 *5.2 Chronology and paleoenvironmental significance of homogenites*

590 According to $^{137}Cs/^{210}Pb$ dating, no discrete layers associated with the 11 fluidization
591 events monitored in B2 during the period 1976-2004 AD (Soler et al., 2007) have been
592 recorded in core BAN-11-1A (Fig. 7). However, a detailed inspection of core images reveals
593 an internal irregular 'sublayering' of mm to sub-mm thick laterally uncontinuous light grey
594 silts within black, massive, carbonate-rich silts of lithotype 1 (Fig. 4A and 8B). These small
595 amounts of light grey silt sediments might be derived from sub-basin B2 and have reached
596 coring site. Therefore, more intense groundwater inflow (or smaller karstic subaqueous
597 springs within sub-basin B2) is required to produce a denser turbidity plume than the ones

598 monitored during the last years (Soler et al., 2007) so that these 17 layers within uppermost
599 unit LC could be deposited. Alternatively, a longer duration for these events could produce
600 thick homogenite layers. However, we would expect some internal structure in the sediment
601 layers if the events lasted several years, and the lack of clear internal structure within these
602 layers make such a long lasting, permanent turbidity plume rather unlikely.

603 The different age models proposed for the uppermost unit containing the homogenites
604 (Fig. 7B), indicate that they were deposited between the 4^{th} and 20^{th} centuries AD.
605 Chronological uncertainties associated with the lack of reliable radiocarbon dates within this
606 interval hamper an accurate dating of these depositional events. In model 1, ^{137}Cs – ^{210}Pb
607 inferred sedimentation rate is unlikely to remain constant throughout several millennia
608 characterized by changing land use and climate. According to model 2, the linear interpolation
609 with the validated date of ~2800 cal yrs BP implies an unlikely abrupt change prior to 1963
610 AD and also a constant sedimentation rate through the intervals containing different
611 lithologies: i) alternating lithotypes 1 and 4 (upper part of the succession) and ii) banded to
612 laminated lithotype 2 (lower part of the succession). Finally, the exclusive validation of the
613 lowermost radiocarbon date within unit LC is arbitrary as all the others were rejected for the
614 potential recycling of material derived from resuspension (Table 2, Fig 7).

615 A fluctuating, long-term increase in lake level in Banyoles is evidenced by the onlapping
616 of unit LC over units LA and LB, containing shallower deposits (Figs. 2 and 3). This is also
617 supported by the existence of a submerged Neolithic settlement in the eastern shore of the
618 lake (La Draga site). This archeological site is constituted by lakeshore type houses dated as
619 old as ~7200 cal. BP (Bosch et al., 2000; Tarrús, 2008), and implies that lake level was up to
620 1.5 m lower than the current level during the Neolithic .

621 A drastic change in depositional environments occurred at the base of Unit C, at ~2.8 cal
622 ka BP, and inaugurated a new lake dynamics favorable to homogenite formation. Although

623 the timing is coherent with a large increase in humidity - particularly in southern Spain
624 (Martín-Puertas et al., 2009) –documented at the onset of the Iberian-Roman Humid Period
625 (ca. 2.5 cal ka BP), moisture conditions have been quite variable during the last 2 millennia in
626 the Iberian Peninsula in general (Moreno et al., 2012) and NE Spain in particular (Morellón et
627 al., 2012). Thus, a direct, exclusive climate driven hydrological change for the deposition of
628 homogenites can be ruled out. However we cannot discard the possibility that changes in the
629 karst functioning with new preferential areas for spring flow brought by the onset of this
630 humid period could have become permanent and favored homogenite formation during the
631 last 3 millennia.

632 The presence of several homogenites at the lowermost part of the recovered sequence,
633 between ~5450 and 7200 cal yrs BP suggest that, apart from the autogenic evolution of these
634 karstic depressions described by Canals et al. (1990), an external hydrological mechanism
635 would be required for such a depositional change. In fact, no homogenites have been
636 identified near to the other sub-basins of the lake by geophysical surveys and sediment cores.
637 Thus, a higher, local groundwater discharge likely caused by a faster recharge of the aquifer
638 might have activated sub-basin B2, causing these episodic, more intense fluidization events
639 and associated turbidity plumes in Lake Banyoles during the last millennia. Without a more
640 detailed age model, the onset of homogenite deposition could have started as early as the
641 humid Iberian-Roman Period or as late as Medieval times. In the second case, it would have
642 been coincident with the human settlement of the area and associated changes in land use and
643 lake hydrology. The foundation of Sant Esteve Monastery in the town of Banyoles (Sanz i
644 Alguacil, 1991) in the early 9^{th} century AD lead to large changes in the lake and the
645 watershed, as the construction of an artificial drainage system (five artificial outlets and
646 several dikes in the eastern shore of the lake) to control lake level. Moreover, intense
647 deforestation and farming affected the catchment drainage and permeability. A local

expansion of agriculture occurred in relation to the foundation of another Romanesque monastery in the town of Besalu (960 AD), located in the recharge area of the aquifer (Sanz, 1981).

Deforestation caused by the important expansion of farmlands in the region and associated increase in soil permeability in the recharge area of the aquifer might have led to a faster recharge of the karstic system feeding Lake Banyoles, increasing its rapid hydrological response to intense rainfall episodes responsible for fluidization episodes in sub-basin B2 and favoring the deposition of homogenites. Higher groundwater inflow through the spring located in sub-basin B2 could be responsible for more intense fluidization events and associated turbidity plumes. Progressive farmland abandonment and associated reforestation during the mid to late 20th century and/or groundwater extraction might have lowered water table, decreasing the intensity of fluidization events in B2 sub-basin during recent times and thus, preventing the deposition of homogenites.

6. Conclusions

Recent sedimentary processes in karstic Lake Banyoles are strongly influenced by the effect of groundwater activity, which leads to fluidization, re-suspension and mainly vertical transport and gravity of sediment particles forming homogenite deposits accumulated in the platforms between deepest sub-basins B1 and B2. These processes are permanent in B1 and periodical in B2, respectively. Based on high-resolution geophysical surveys and detailed sedimentological and geochemical analyses of several cores, we document a large variability in the intensity and frequency of these transport processes and the subsequent deposition of homogenite layers during the last millennia.

The ~7.6 cal kyr BP recovered sequence of Lake Banyoles has recorded an increase in lake level after ~2800 cal yrs BP, as indicated by geophysical (i.e., the onlapping of

673 uppermost unit SC onto lowermost units SA and SB) and sedimentological (i.e., change from
674 massive, carbonate-rich shallow lake deposits into fine-grained, clastic-rich sediments)
675 evidences. This lake level change was accompanied by a subsequent intensification of
676 groundwater input and the deposition of up to 75 cm thick 17 layers of homogenites.

677 Textural and compositional analysis and depositional patterns of homogenites indicate
678 that they have been deposited by periodical, intense, fluidization events in sub-basin B2 as
679 those described and monitored for recent times. Intensity, however, was higher, able to
680 generate thicker, discrete layers in marginal areas of the platform between the deepest sub-
681 basins in the southern basin of the lake. The onset of these events was triggered by higher and
682 more intense local, groundwater inflow and might be related to agricultural expansion during
683 Roman and/or medieval times in the region. Increased farmland surface in the recharge area
684 of the aquifer increased soil permeability and subsequently, the rapid response of the aquifer
685 to intense rainfall episodes in the recharge area.

686

687 **Acknowledgements**

688 Financial support for research was provided by the Spanish Inter-Ministry
689 Commission of Science and Technology (CICYT), through the projects GLOBALKARST
690 (CGL2009-08415) and GRACCIE-CONSOLIDER (CSD2007-00067). Additional funding
691 was provided by INTIMATE-COST through a travel grant 'Short Term Scientific Mission,
692 COST Action ES0907' in 2011 at IPE-CSIC and University of Barcelona (Spain).

693 M. Morellón and F. Barreiro hold 'JAE-DOC' and 'JAE-PREDOC' pre and
694 postdoctoral contracts, respectively, both co-funded by C.S.I.C. and the European Social
695 Fund. We acknowledge the Town Hall of Banyoles (Girona) and Club Natació Banyoles for
696 their collaboration in fieldwork activities and Jaime Frigola and Pol Tarrats (Univ. of
697 Barcelona), and Miguel Sevilla and Josu Aranbarri (IPE-CSIC) for coring assistance in 2011.

We are also grateful to Irene Brunner, Silvia Bollhalder, Marian Fujak, Alois Zwyssig and Brian Sinnet (Eawag, Switzerland); Adrian Gilli and Stephanie Wirth (ETH-Zürich, Switzerland) and Beatriz Bueno, Aida Adsuar and Miguel Bartolomé (IPE-CSIC, Spain) for their laboratory assistance and collaboration in this research. We thank constructive comments on the manuscript made by Maria Rieradevall (Univ. of Barcelona).

REFERENCES

Álvarez-Cobelas, M., Rojo, C., Angeler, D.G., 2005. Mediterranean limnology: current status, gaps and the future. Journal of Limnology, 64(1): 13-29.

Assayag, N., Jézéquel, D., Ader, M., Viollier, E., Michard, G., Prévot, F., Agrinier, P., 2008. Hydrological budget, carbon sources and biogeochemical processes in Lac Pavin (France): Constraints from $\delta^{18}O$ of water and $\delta^{13}C$ of dissolved inorganic carbon. Applied Geochemistry, 23(10): 2800-2816.

Barnolas, A., 1992. Evolución sedimentaria de la Cuenca Surpirenaica Oriental durante el Eoceno. Acta Geologica Hispanica, 27(1-2): 15-31.

Beck, C., 2009. "Late Quaternary lacustrine paleo-seismic archives in north-western Alps: Examples of earthquake-origin assessment of sedimentary disturbances". Earth-Science Reviews, 96(4): 327-344.

Bischoff, J.L., Julià, R., Shanks, W.C., Rosenbauer, R.J., 1994. Karstification without carbonic acid: Bedrock dissolution by gypsum-driven dedolomitization. Geology, 22(11): 995-998.

Bloesch, J., 1995. Mechanisms, measurement and importance of sediment resuspension in lakes. Marine and Freshwater Research, 46(1): 295-304.

722 Bosch, A., Chinchilla, J., Tarrús, J., 2000. El Poblat Lacustre Neolitic de la Draga:
723 Excavaciones de 1990 a 1998. Museu d'Arqueologia de Catalunya-Centre
724 d'Arqueologia Subaquàtica de Catalunya, Girona, Girona (Spain).
725 Brusi, D., Bach, J., Sanz, M., 1990. Itinerari geològic de Banyoles. Descoberta del
726 funcionament del sistema lacustre. Apunts 22. Eumo Editorial, Barcelona, 124 pp.
727 Burbank, D.W., Puigdefàbregas, C., Muñoz, J.A., 1992. The chronology of the Eocene
728 tectonic and stratigraphic development of the eastern Pyrenean foreland basin,
729 northeast Spain. Geological Society of America Bulletin, 104(9): 1101-1120.
730 Burne, R.V., Moore, L.S., 1987. Microbialites; organosedimentary deposits of benthic
731 microbial communities. PALAIOS, 2(3): 241-254.
732 Canals, M., Got, H., Julia, R., Serra, J., 1990. Solution-collapse depressions and suspensates
733 in the limnocrenic lake of Banyoles (NE Spain). Earth Surface Processes and
734 Landforms, 15(3): 243-254.
735 Casamitjana, X., Colomer, J., Roget, E., Serra, T., 2006. Physical Limnology in Lake
736 Banyoles. Limnetica, 25(1-2): 181-188.
737 Casamitjana, X., Colomer, J., Roget, E., Teresa, S., 1996. On the presence of aggregates in
738 the basins of Lake Banyoles. Geophysical Research Letters, 23(20): 2737-2740.
739 Casamitjana, X., Roget, E., 1993. Resuspension of sediment by focused groundwater in Lake
740 Banyoles. Limnology and Oceanography, 38(3): 643-656.
741 Colomer, J., Ross, J.A., Casamitjana, X., 1998. Sediment entrainment in karst basins. Aquatic
742 Sciences, 60(4): 338-358.
743 Colomer, J., Serra, T., Piera, J., Roget, E., Casamitjana, X., 2001. Observations of a
744 hydrothermal plume in a karstic lake. Limnology and Oceanography, 46(1): 197-203.
745 Colomer, J., Serra, T., Soler, M., Casamitjana, X., 2002. Sediment fluidization events in a
746 lake caused by large monthly rainfalls. Geophys. Res. Lett., 29(8): 1260.

747 Coma, M.V., Abella, C.A., Oromi, O., 1988. Caracteritzacio fisico-quimica dels travertins en
748 formació de l'Estany de Banyoles. Scientia gerundensis, 14: 43-56.
749 Coma, M.V., Oromi, O., Abella, C.A., 1987. Cartografia dels travertins en formació de
750 l'Estany de Banyoles. Scientia gerundensis, 13: 65-74.
751 Cho Martínez, S., 2012. Registros sedimentarios como indicadores paleoambientales y de
752 actividad antrópica en el Neolítico del Lago de Banyoles. Master Thesis, Universidad
753 de Burgos Burgos (Spain), 48 pp.
754 Chung, F.H., 1974a. Quantitative interpretation of X-ray diffraction patterns of mixtures. I.
755 Matrix-flushing method for quantitative multicomponent analysis. Journal of Applied
756 Crystallography, 7(519-525).
757 Chung, F.H., 1974b. Quantitative interpretation of X-ray diffraction patterns of mixtures. II.
758 Adiabatic principle of X-ray diffraction analysis of mixtures. Journal of Applied
759 Crystallography, 7: 526-531.
760 Dadheech, P.K., Glöckner, G., Casper, P., Kotut, K., Mazzoni, C.J., Mbedi, S., Krienitz, L.,
761 2013. Cyanobacterial diversity in the hot spring, pelagic and benthic habitats of a
762 tropical soda lake. FEMS Microbiology Ecology, 85(2): 389-401.
763 Descy, J.-P., Darchambeau, F., Schmid, M., 2012a. Lake Kivu Research: Conclusions and
764 Perspectives. In: J.-P. Descy, F. Darchambeau, M. Schmid (Eds.), Lake Kivu. Aquatic
765 Ecology Series. Springer Netherlands, pp. 181-190.
766 Descy, J.-P., Darchambeau, F., Schmid, M. (Eds.), 2012b. Lake Kivu. Limnology and
767 biogeochemistry of a tropical great lake. Aquatic Ecology Series, 5. Springer.
768 Draganits, E., Janda, C., 2003. Subaqueous artesian springs and associated spring pits in a
769 Himalayan pond. Boreas, 32(2): 436-442.
770 Dutras, A., Abella, C., Brunet, R., 1986. Determinació del sistema de corrents a l'Estany de
771 Banyoles en condiciones de calma meteorològica estival. In: D.d. Girona (Ed.),

772 Primeres jornades sobre l'Estany de Banyoles. Ponències i comunicacions, Banyoles
773 (Spain), pp. 149-157.
774 Edmunds, W.M., Dodo, A., Djoret, D., Gaye, C., Goni, I., Travi, Y., Zouari, K., Zuppi, G.-
775 M., Gasse, F., 2004. Groundwater as an archive of climatic and environmental change:
776 Europe to Africa. In: R. Battarbee, F. Gasse, C. Stickley (Eds.), Past Climate
777 Variability through Europe and Africa. Developments in Paleoenvironmental
778 Research. Springer Netherlands, pp. 279-306.
779 Garcia-Gil, L.J., Borrego, C.M., Bañeras, L., Abella, C.A., 1993. Dynamics of Phototrophic
780 Microbial Populations in the Chemocline of a Meromictic Basin of Lake Banyoles.
781 Internationale Revue der gesamten Hydrobiologie und Hydrographie, 78(2): 283-294.
782 García-Ruiz, J.M., López-Moreno, J.I., Vicente-Serrano, S.M., Lasanta-Martínez, T.,
783 Beguería, S., 2011. Mediterranean water resources in a global change scenario. Earth-
784 Science Reviews, 105(3-4): 121-139.
785 Girardclos, S., Schmidt, O.T., Sturm, M., Ariztegui, D., Pugin, A., Anselmetti, F.S., 2007.
786 The 1996 AD delta collapse and large turbidite in Lake Brienz. Marine Geology,
787 241(1-4): 137-154.
788 Guerrero, R., Abella, C., Miracle, M.R., 1978. Spatial and temporal distribution of bacteria in
789 a meromictic karstic lake basin: relationships with physicochemical parameters and
790 zooplankton. Verhandlungen des Internationalen Verein Limnologie, 20(2264-2271).
791 Höbig, N., Weber, M.E., Kehl, M., Weniger, G.-C., Julià, R., Melles, M., Fülöp, R.-H.,
792 Vogel, H., Reicherter, K., 2012. Lake Banyoles (northeastern Spain): A Last Glacial to
793 Holocene multi-proxy study with regard to environmental variability and human
794 occupation. Quaternary International, 274(0): 205-218.
795 Hsü, K.J., Kelts, K., 1985. Swiss lakes as a geological laboratory. Naturwissenschaften, 72(6):
796 315-321.

797 Ionescu, D., Siebert, C., Polerecky, L., Munwes, Y.Y., Lott, C., Häusler, S., Bižić-Ionescu,
798 M., Quast, C., Peplies, J., Glöckner, F.O., Ramette, A., Rödiger, T., Dittmar, T., Oren,
799 A., Geyer, S., Stärk, H.-J., Sauter, M., Licha, T., Laronne, J.B., de Beer, D., 2012.
800 Microbial and Chemical Characterization of Underwater Fresh Water Springs in the
801 Dead Sea. PLoS ONE, 7(6): e38319.
802 Julià-Brugués, R., 1977. Nuevos datos sobre la posicion cronoestratigráfica de los materiales
803 cuaternarios de la cuenca lacustre de Banyoles-Besalú (Girona). Acta Geológica
804 Hispánica XII(1-3): 55-59.
805 Julia Bruguès, R., Suc, J.-P., 1980. Analyse pollinique des dépôts lacustresdu Pléistocène
806 inférieur de Banyoles (Bañolas, site de la Bòbila Ordis - Espagne): un élément
807 nouveau dans la reconstitution de l'histoire paléoclimatique des régions
808 méditerranéennes d'Europe occidentale. Geobios, 13(1): 5-19.
809 Julià, R., 1980. La conca lacustre de Banyoles Centro d'Estudios Comarcals de Banyoles,
810 Besalu, 188 pp.
811 Julià, R., Bischoff, J.L., 1991. Radiometric dating of quaternary deposits and the hominid
812 mandible of lake banyolas, Spain. Journal of Archaeological Science, 18(6): 707-722.
813 Leroy, S.A.G., 1997. Climatic and non-climatic lake-level changes inferred from a Plio-
814 Pleistocene lacustrine complex of Catalonia (Spain): palynology of the Tres Pins
815 sequences. Journal of Paleolimnology, 17(4): 347-367.
816 Løvlie, R., Leroy, S., 1995. Magnetostratigraphy of Lower Pleistocene Banyoles palaeolake
817 carbonate sediments from Catalonia, NE Spain: Evidence for relocation of the Cobb
818 Mountain sub-chron. Quaternary Science Reviews, 14(5): 473-485.
819 MAGRAMA, 2006. Information Sheet on Ramsar Wetlands: Lake Banyoles, pp. 21.
820 Martín-Puertas, C., Valero-Garcés, B.L., Brauer, A., Mata, M.P., Delgado-Huertas, A.,
821 Dulski, P., 2009. The Iberian-Roman Humid Period (2600-1600 cal yr BP) in the

822 Zoñar Lake varve record (Andalucía, southern Spain). Quaternary Research, 71(2):
823 108-120.
824 Mató i Palós, E., Saula i Briansó, E., Picart i Boira, J., Solà i Subiranas, J., Montaner i
825 Roviras, J., Viñals i Gisbert, E., Samsó i Escolá, J.M., Serra i Kiel, J., Llenas i
826 Abellaneda, M., Agustí i Ballester, J., Mallarach i Carrera, J., 1996. Banyoles 295-2-1
827 (76,23). In: X. Berástegui Batalla, M. Losantos Sistach, J. Cirés (Eds.), Mapa geològic
828 de Catalunya 1:25000. Generalitat de Catalunya, Departament de Politica Territorial i
829 Obres Públiques, Institut Cartográfic de Catalunya, Servei Geològic de Catalunya,
830 Barcelona (Spain).
831 Matter, M., Anselmetti, F.S., Jordanoska, B., Wagner, B., Wessels, M., Wüest, A., 2010.
832 Carbonate sedimentation and effects of eutrophication observed at the Kališta
833 subaquatic springs in Lake Ohrid (Macedonia). Biogeosciences, 7(11): 3755-3767.
834 Morellón, M., Pérez-Sanz, A., Corella, J.P., Büntgen, U., Catalán, J., González-Sampériz, P.,
835 González-Trueba, J.J., López-Sáez, J.A., Moreno, A., Pla-Rabes, S., Saz-Sánchez,
836 M.Á., Scussolini, P., Serrano, E., Steinhilber, F., Stefanova, V., Vegas-Vilarrúbia, T.,
837 Valero-Garcés, B., 2012. A multi-proxy perspective on millennium-long climate
838 variability in the Southern Pyrenees. Clim. Past, 8(2): 683-700.
839 Morellón, M., Valero-Garcés, B., Anselmetti, F., Ariztegui, D., Schnellmann, M., Moreno, A.,
840 Mata, P., Rico, M., Corella, J.P., 2009. Late Quaternary deposition and facies model
841 for karstic Lake Estanya (North-eastern Spain). Sedimentology, 56(5): 1505-1534.
842 Moreno-Amich, R., García-Berthou, E., 1989. A new bathymetric map based on echo-
843 sounding and morphometrical characterization of the Lake of Banyoles (NE-Spain).
844 Hydrobiologia, 185: 83-90.
845 Moreno, A., Pérez, A., Frigola, J., Nieto-Moreno, V., Rodrigo-Gámiz, M., Martrat, B.,
846 González-Sampériz, P., Morellón, M., Martín-Puertas, C., Corella, J.P., Belmonte, Á.,

847 Sancho, C., Cacho, I., Herrera, G., Canals, M., Grimalt, J.O., Jiménez-Espejo, F.,
848 Martínez-Ruiz, F., Vegas-Vilarrúbia, T., Valero-Garcés, B.L., 2012. The Medieval
849 Climate Anomaly in the Iberian Peninsula reconstructed from marine and lake records.
850 Quaternary Science Reviews, 43(0): 16-32.
851 Olivera, C., Redondo, E., Lambert, J., Riera, A., Roca, A., 2006. Els terratrèmols dels segles
852 XIV i XV a Catalunya. Institut Cartogràfic de Catalunya, Barcelona.
853 Paillard, D., Labeyrie, L., Yiou, P., 1996. Analyseries 1.0: a Macintosh software for the
854 analysis of geographical time-series. Eos, 77: 379.
855 Pérez-Obiol, R., Julià, R., 1994. Climatic Change on the Iberian Peninsula Recorded in a
856 30,000-Yr Pollen Record from Lake Banyoles. Quaternary Research, 41(1): 91-98.
857 Prat, N., Rieradevall, M., 1995. Life cycle and production of Chironomidae (Diptera) from
858 Lake Banyoles (NE Spain). Freshwater Biology, 33(3): 511-524.
859 Reimer, P.J., Baillie, M.G.L., Bard, E., Bayliss, A., Beck, J.W., Blackwell, P.G., Ramsey,
860 C.B., Buck, C.E., Burr, G.S., Edwards, R.L., Friedrich, M., Grootes, P.M., Guilderson,
861 T.P., Hajdas, I., Heaton, T.J., Hogg, A.G., Hughen, K.A., Kaiser, K.F., Kromer, B.,
862 McCormac, F.G., Manning, S.W., Reimer, R.W., Richards, D.A., Southon, J.R.,
863 Talamo, S., Turney, C.S.M., van der Plicht, J., Weyhenmeyer, C.E., 2009. IntCal09
864 and Marine09 Radiocarbon Age Calibration Curves, 0-50,000 Years cal BP.
865 Radiocarbon, 51(4): 1111–1150.
866 Rieradevall, M., Roca, J.R., 1995. Distribution and population dynamics of ostracodes in a
867 Karstic lake: Lake Banyoles (Catalonia, Spain). Hidrobiología, 310(3): 189-196.
868 Roget, E., Colomer, J., Casamitjana, X., Llebot, J.E., 1993. Bottom currents induced by
869 baroclinic forcing in Lake Banyoles (Spain). Aquatic Sciences - Research Across
870 Boundaries, 55(3): 206-227.

871 Rosen, M.R., Arehart, G.B., Lico, M.S., 2004. Exceptionally fast growth rate of <100-yr-old
872 tufa, Big Soda Lake, Nevada: Implications for using tufa as a paleoclimate proxy.
873 Geology, 32(5): 409-412.
874 Rosen, M.R., Chagué-Goff, C., Eser, P., Coshell, L., 2002. Utilisation of the sedimentological
875 and hydrochemical dynamics of the Stump Bay Wetland along Lake Taupo, New
876 Zealand, for the recognition of paleo-shoreline indicators. Sedimentary Geology,
877 148(1–2): 357-371.
878 Ross, K.A., Smets, B., De Batist, M., Schmid, M., Anselmetti, F.S., in review.
879 Morphobathymetry of Lake Kivu and its implications for lake-level history,
880 subaquatic volcanism and natural hazard assessment. Earth and Planetary Science
881 Letters.
882 Sanz i Alguacil, A., 1991. Catalunya Romanica. Vol V. El Gironès, la Selva, el Pla de
883 l'Estany, Enciclopèdia Catalana.
884 Sanz, M., 1981. El sistema hidrogeológico de Banyoles-La Garrotxa. Unpublished PhD thesis,
885 Universitat Autònoma de Barcelona, Barcelona, Spain.
886 Saula, E., Picart, J., Mato, E., Llenas, M., Lozanitos, M., Beràstegui, X., Agustí, J., 1994.
887 Evolución geodinámica de la fosa del Empordà y las Sierras Transversales. Acta
888 Geologica Hispanica, 29(2-4): 55-75.
889 Schnellmann, M., Anselmetti, F.S., Giardini, D., McKenzie, J.A., 2005. Mass movement-
890 induced fold-and-thrust belt structures in unconsolidated sediments in Lake Lucerne
891 (Switzerland). Sedimentology, 52(2): 271-289.
892 Schnurrenberger, D., Russell, J., Kelts, K., 2003. Classification of lacustrine sediments based
893 on sedimentary components. Journal of Paleolimnology, 29: 141-154.

894 Secanell, R., Goula, X., Susagna, T., Fleta, J., Roca, A., 2004. Seismic hazard zonation of
895 Catalonia, Spain, integrating random uncertainties. Journal of Seismology, 8(1): 25-
896 40.
897 Serra-Kiel, J., Travé, A., Mató, E., Saula, E., Ferràndez-Cañadell, C., Busquets, P., Tosquella,
898 J., Vergés, J., 2003. Marine and Transitional Middle/Upper Eocene Units of the
899 Southeastern Pyrenean Foreland Basin (NE Spain). Geologica Acta, 1(2): 177-200.
900 Serra, T., Colomer, J., Gacia, E., Soler, M., Casamitjana, X., 2002. Effects of a turbid
901 hydrothermal plume on the sedimentation rates in a karstic lake. Geophys. Res. Lett.,
902 29(21): 2029.
903 Serra, T., Soler, M., Julià, R., Casamitjana, X., Colomer, J., 2005. Behaviour and dynamics of
904 a hydrothermal plume in Lake Banyoles, Catalonia, NE Spain. Sedimentology, 52(4):
905 795-808.
906 Shapley, M.D., Ito, E., Donovan, J.J., 2005. Authigenic calcium carbonate flux in
907 groundwater-controlled lakes: Implications for lacustrine paleoclimate records.
908 Geochimica et Cosmochimica Acta, 69(10): 2517-2533.
909 Soler, M., Serra, T., Casamitjana, X., Colomer, J., 2009. High sedimentation rates in a karstic
910 lake associated with hydrothermal turbid plumes (Lake Banyoles, Catalonia, NE
911 Spain). Sedimentary Geology, 222(1-2): 5-15.
912 Soler, M., Serra, T., Colomer, J., Romero, R., 2007. Anomalous rainfall and associated
913 atmospheric circulation in the northeast Spanish Mediterranean area and its
914 relationship to sediment fluidization events in a lake. Water Resour. Res., 43(1):
915 W01404.
916 Tarrús, J., 2008. La Draga (Banyoles, Catalonia), an Early Neolithic Lakeside Village in
917 Mediterranean Europe. Catalan historical review, 1: 17-33.

Tassone, A., Roca, E., Muñoz, J.A., Cabrera, L., Canals, M., 1994. Evolución del sector septentrional del margen continental catalán durante el Cenozoico Acta Geologica Hispanica, 29(2-4): 3-7.

Valero- Garcés, B., Morellón, M., Moreno, A., Corella, P., Martín-Puertas, C., Barreiro, F., Pérez, A., Giralt, S., Mata-Campo, M.P., 2013. The carbonate factory in karst lakes: sources, processes and depositional environments in Quaternary Iberian Lakes. Sedimentary Geology, in press.

Valero-Garcés, B., Zeroual, E., Kelts, K., 1998. Arid phases in the Western Mediterranean Region during the last glacial cycle reconstructed from lacustrine records. In: G. Benito, Baker, V.R., Gregory, K.J. (Ed.), Palaeohydrology and Environmental Change. John Wiley & Sons Ltd., pp. 67-80.

Warren, J.K., 1982. The hydrological significance of Holocene tepees, stromatolites, and boxwork limestones in coastal salinas in South Australia. Journal of Sedimentary Research, 52(4): 1171-1201.

Winter, T.C., 1999. Relation of streams, lakes, and wetlands to groundwater flow systems. Hydrogeology Journal, 7(1): 28-45.

Younger, P.L., Teutsch, G., Custodio, E., Elliot, T., Manzano, M., Sauter, M., 2002. Assessments of the sensitivity to climate change of flow and natural water quality in four major carbonate aquifers of Europe. Geological Society, London, Special Publications, 193(1): 303-323.

TABLE CAPTIONS

	Lithotype	*Sedimentological features*	*Compositional parameters*	*Depositional subenvironment/ process*
Banded and laminated	**1**	***Dark-grey to black, massive to banded, carbonate-rich silts with diatoms*** Fine grained carbonate mud composed by up to 10 µm hexagonal calcite grains with abundant to frequent ca. 50-60 µm reworked occasional reworked littoral carbonate-rich particles (ostracods, charophytes and carbonate coatings). Frequent ca. 25 µm detrital carbonate particles, plant remains and diatoms, locally abundant. Occasional quartz grains and < 20µm pyrite framboids.	**TIC** = 3.3% - 6.7 % **TOC** = 0.0% - 1.2 % **Mean GS** = 5 – 18 µm **Mineralogy**: **Cc**= 42.3%, **Ill** = 32.5%, **Chl**= 17.7%, **Qtz**= 7.4%	Deep, monomictic, occasionally anoxic brackish to freshwater lake with permanent, low-concentration turbidity plumes
	2	***Laminated fcs comprising alternating mm to 1 cm thick black and light-grey fine-grained silts*** Black laminae: Fine-grained (up to 10 µm) hexagonal to sub-hexagonal calcite grains with abundant diatoms, up to 100 µm reworked littoral carbonate particles and frequent 20-30 µm detrital grains of quartz and carbonates. Light grey laminae: fine-grained, up to 10 µm irregular, reworked calcite crystals with frequent up to 40 µm clastic quartz and non-biogenic carbonates. Occasional to frequent up to 50 µm reworked littoral carbonate-rich particles.	**TIC =** 3.9 % – 6.2 % **TOC** = 0.2 %- 1.1 % **Mean GS =** 6.0 – 8.4 µm **Mineralogy: Cc** = 39.5%, **Ill** = 32.7%, **Chl** = 19.5%, **Qtz** = 8.2%	Relatively deep, carbonate-producing lake with seasonal anoxic hypolimnetic conditions
	3	***Grey, barely laminated to massive, carbonate-rich silts with evidences of bioturbation*** 30-50 µm reworked biogenic carbonate particles with abundant up to 50 µm irregularly shaped detrital grains of quartz and carbonates. Frequent fine-grained, up to 10 µm calcitic mud.	**TIC =** 4.4% – 9.3% **TOC** = 0.3%- 1.0 % **Mean GS** =4.8 – 18.9 µm **Mineralogy: Cc** = 51.6%, **Ill** = 26.5%, **Chl** = 15.1%, **Qtz** = 6.9%	Shallow, carbonate-producing brackish lake with oxic conditions
Massive	**4**	***Light grey, massive fine-grained, carbonate-rich silts, occurring as mm to cm-thick intercalations or cm to dm-thick homogeneous layers*** Up to 10 µm fine-grained irregularly-shaped calcite mud with abundant reworked diatoms. Frequent up to 50 µm reworked carbonate particles, sub-circular calcareous algae and pyrite framboids. Occasional plant remains.	**TIC =** 4.3% -6.8 % **TOC** = 0.1% - 0.9 % **Mean GS =** 5 – 12.6 µm **Mineralogy: Cc** = 44.7%, **Ill** = 31.7%, **Chl** = 16.2%, **Qtz** = 7.4%	Fluidization events and associated periodical and intense turbidity plumes

5	***Light grey/yellowish, massive, fine-grained, up to 1 m thick fining upwards sequences ranging from coarse to fine-grained silts*** Dominant 10-15 µm reworked, sub-rounded to hexagonal calcite grains with reworked littoral carbonate-rich particles (up to 50-60 µm), more frequent towards the base.	**TIC** = 4.5 % - 7.3% **TOC** = 0.3 % - 0.6 % **Mean GS** = 8.2 – 13.0 µm **Mineralogy: Cc** = 40.9%, **Ill** = 32.7%, **Chl** = 18.8%, **Qtz** = 7.7%	Mass-wasting processes
6	***Light grey/yellowish, massive, fine-grained, carbonate-rich sands*** 100-300 µm sub-rounded, biogenic, reworked carbonate particles with abundant up to 100 µm coarse, high relief detrital grains of quartz and non-biogenic carbonates. Abundant fine-grained matrix composed of up to 10 µm sub-rounded calcite crystals.	**TIC** = 7.2% - 8.8% **TOC** = 0.4% - 0.5 % **Mean GS** = 65.5 µm **Mineralogy: Cc** = 57.9%, **Chl** = 18.1%, **Ill** = 15.4%, **Qtz** = 8.6%	Mass-wasting processes

Table 1. Lithotypes defined for the Lake Banyoles sequence, including sedimentological features, main compositional parameters (TIC = Total Inorganic Carbon, TOC = Total Organic Carbon, GS = Grain Size and mineralogical content (%), including: quartz (Qtz), chlorite (Chl), illite (Ill) and calcite (Cc)) and depositional subenvironments and/or process interpreted for each case.

Comp depth (cm)	*Unit*	*Laboratory code*	*Type of material*	*AMS ^{14}C age (yr B.P.)*	*Corrected AMS ^{14}C age*	*Calibrated corrected age (cal yrs BP) (2σ range)*
44,5	LC	D-AMS 001611	Bulk organic matter	5460 ± 35	-13 ± 35	*Modern*
123	LC	D-AMS 001114	Bulk organic matter	6537 ± 36	1064 ± 71	984 ± 187
197,7	LC	D-AMS 001113	Bulk organic matter	5441 ± 33	-32 ± 68	*Modern*
290,5	LC	D-AMS 001609	Bulk organic matter	6519 ± 31	1046 ± 66	979 ± 187
528,8	LC	D-AMS 001112	Bulk organic matter	6217 ± 52	744 ± 87	723 ± 179
627,2	LB	D-AMS 001111	Bulk organic matter	5743 ± 39	2718 ± 324	2808 ± 802
996,1	LA	D-AMS 001610	Bulk organic matter	7813 ± 40	4788 ± 325	5453 ± 824
1297,9	LA	D-AMS 001110	Bulk organic matter	9790 ± 54	6765 ± 339	7600 ± 580
1297,9	LA	ETH-45854	Charcoal	6765 ± 285	6765 ± 285	7600 ± 580

Table 2. Radiocarbon dates used for the construction of the age model for the Lake Banyoles sequence. A correction of 3025 ± 35 ^{14}C years was applied to bulk sediment samples from units LA and LB, and 5473 ± 285 ^{14}C years to uppermost lithological unit LC. Corrected dates were calibrated using CALIB 6.0 software and the INTCAL09 curve (Reimer et al., 2009); and the mid-point of 95.4% (2σ probability interval) was selected.

FIGURE CAPTIONS

Fig. 1. (A) Location of the Lake Banyoles within the Iberian Peninsula; (B) bathymetric map, basins and sub-basins (modified from Soler et al., 2009); (C) aerial photograph with seismic grids obtained with the Pinger 3.5 KhZ source (yellow) and Edgetech profiler (red), with indication of the seismic profile displayed below, long (dots) and short core (squares) locations; and (D) N-S seismic profile.

Fig. 2. (A) W-E seismic section (line 4) and correlation with core BAN-11-1A indicated by superposition of core image, sedimentological profile (see legend below) and density profile (g/cm^3); (B) S-N seismic section (line 24) with core BAN-11-1A location and limits of seismic units marked by blue dotted lines; (C) Location of (A) and (B) in the seismic grid.

Fig. 3. Composite sequence for Lake Banyoles record (core BAN-11-1A). From left to right: core image, sedimentary units, sedimentological profile (see legend in Fig. 2 and lithotypes description in Table 1), lightness record (L*), magnetic susceptibility (MS) (SI units), total inorganic carbon (TIC), total organic carbon (TOC) (%), mineralogical composition (%), including: quartz (Qtz), chlorite (Chl), illite (Ill) and calcite (Cc) (see legend below); mean and mode grain size (μm) and grain size classes (sand, silt and clay) distribution (%) (see legend below). Homogenites and turbidite event layers are indicated by horizontal blue and orange bands, respectively.

Fig. 4: High resolution core images of the different lithotypes defined for the Lake Banyoles sequence: A, lithotype 1; B, lithotype 2; C, lithotype 3; D, lithotype 4; E,

alternation between lithotypes 1 and 4; F, turbidite sequence composed by lithotypes 6 (base) and 5 (mid-top of the core section); G, suspended sediments within sub-basin B1; and H, suspended sediments within sub-basin B2.

Fig. 5. Backscattered scanning electron images in selected intervals of cores BAN-11-1A, BAN-12-1 and 2. (A-C) Lithotype 1: (A) General view (3000x), (B) detail of endogenic carbonates (12000x), (C) detail of detrital grains and plant remains transported from the watershed (6000x). (D-F) Lithotype 4 (homogenites): (D) General view (3000x), (E) detail of a pyrite framboid (12000x), (F) detail of coccolithophorid remains transported from the calcareous bedrock of deepest sub-basin and reworked diatoms (12000x).

Fig. 6. (A) X-ray Fluorescence (XRF) scanner data of lithologic Unit LC. Element concentrations (Al, Si, Ti, Fe, Mn, Ca, Sr, S), expressed as counts per second, and Ti/Ca, Sr/Ca and Fe/Mn ratios are indicated. Core image, sedimentary units and sedimentological profile are also included (see legend in Fig. 2). Homogenites are indicated by horizontal blue bands. (B) Bipolar plot of Ca vs. Ti relationship along lithotypes 4 (homogenites), 1 and suspended sediments from short gravity cores BAN-11-1 and 2.

Fig. 7. (A) Chronological model of the composite sequence of Lake Banyoles, formed by long cores BAN-11-1A and short core 1A-1G, based on the linear interpolation of AMS ^{14}C dates (black and white dots) and 1963 AD maximum ^{137}Cs peak (star). Material used for dating and rejected dates are also indicated in the legend. Different models proposed for the uppermost part (1, 2 and 3) correspond to red, green and blue

lines, respectively. Homogenites and turbidite event layers are indicated by horizontal blue and orange bands, respectively. (B) ^{137}Cs and ^{210}Pb activity profiles for the uppermost 70 cm of the sequence. (C) Detail of age/depth relationships along the uppermost unit C.

Fig. 8. (A) Interpreted composite seismic profile between deepest sub-basins B1 and B2 with the location of short and long cores and interpreted deposits of homogenites derived from B1 (orange) and B2 (blue) sub-basins. (B) Correlation panel of short gravity cores (BAN-12-1, 2, 3, 4, 5, 6 and 8) and long core BAN-11-1A along a transect between sub-basins B1 and B2. Orange and blue-shaded areas represent correlation between homogenites derived from B1 and B2, respectively. (C) Core locations on the seismic grid in an aerial photograph of Lake Banyoles.

Figure 1

Click here to download high resolution image

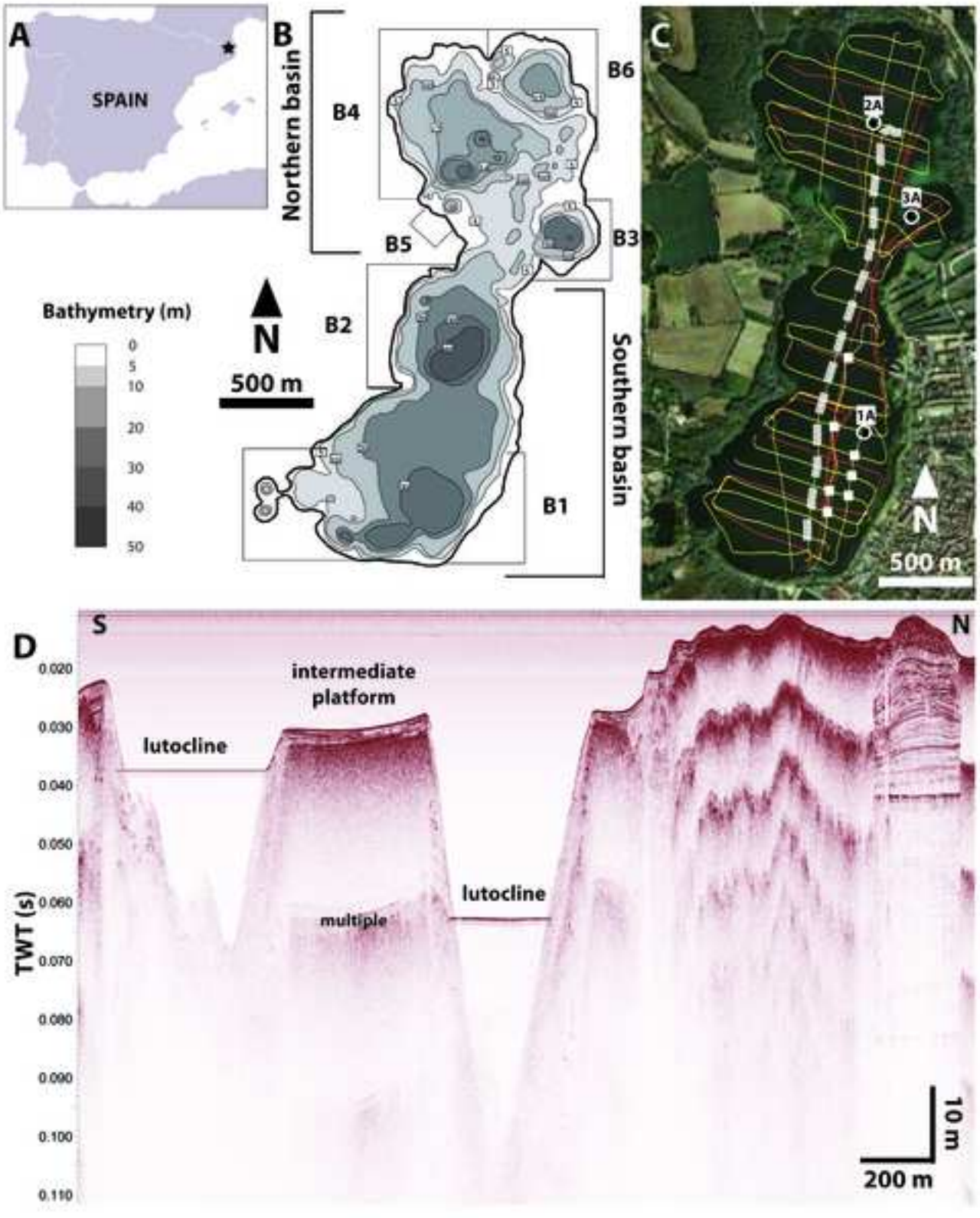

Figure 2

Click here to download high resolution image

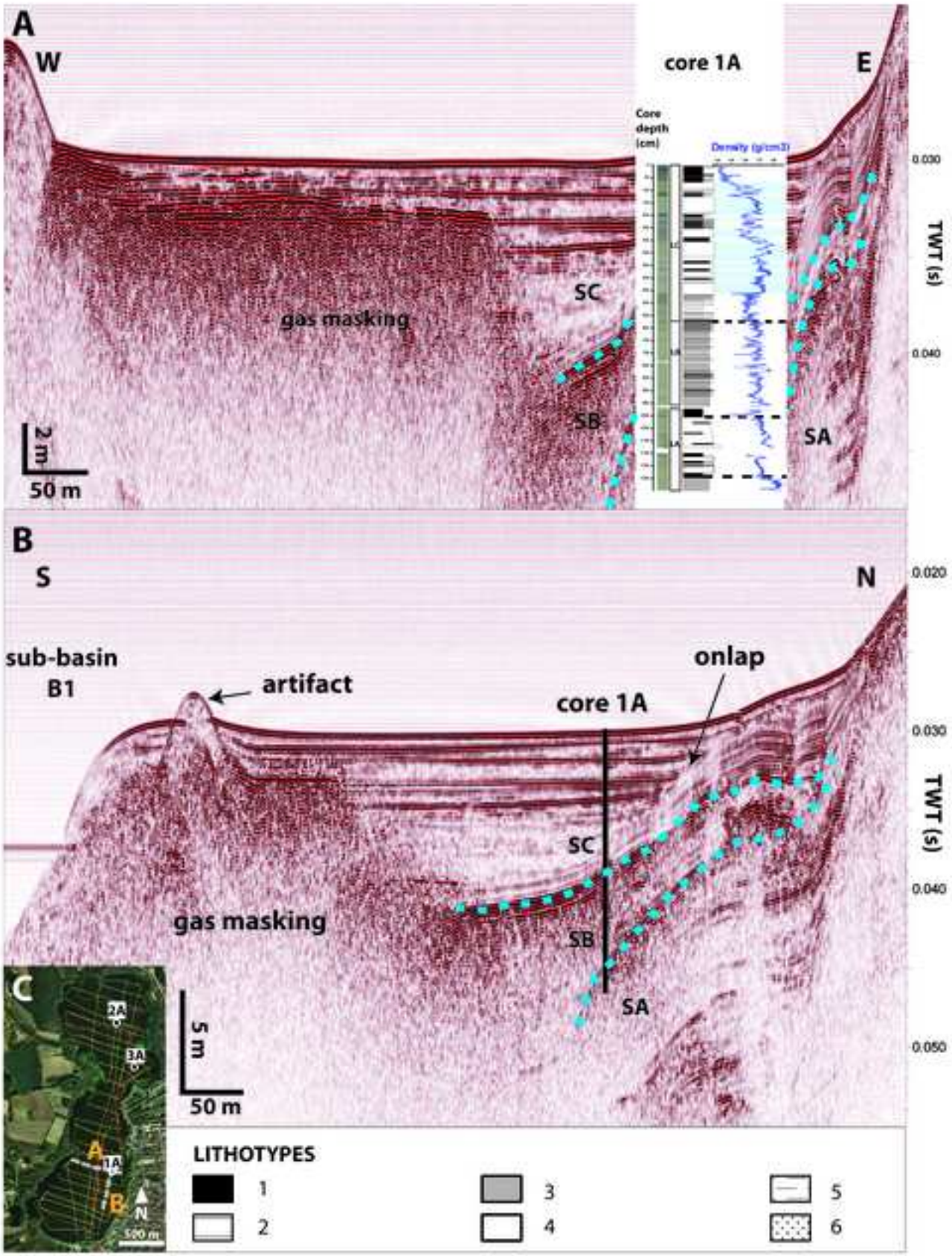

Figure 3

Click here to download high resolution image

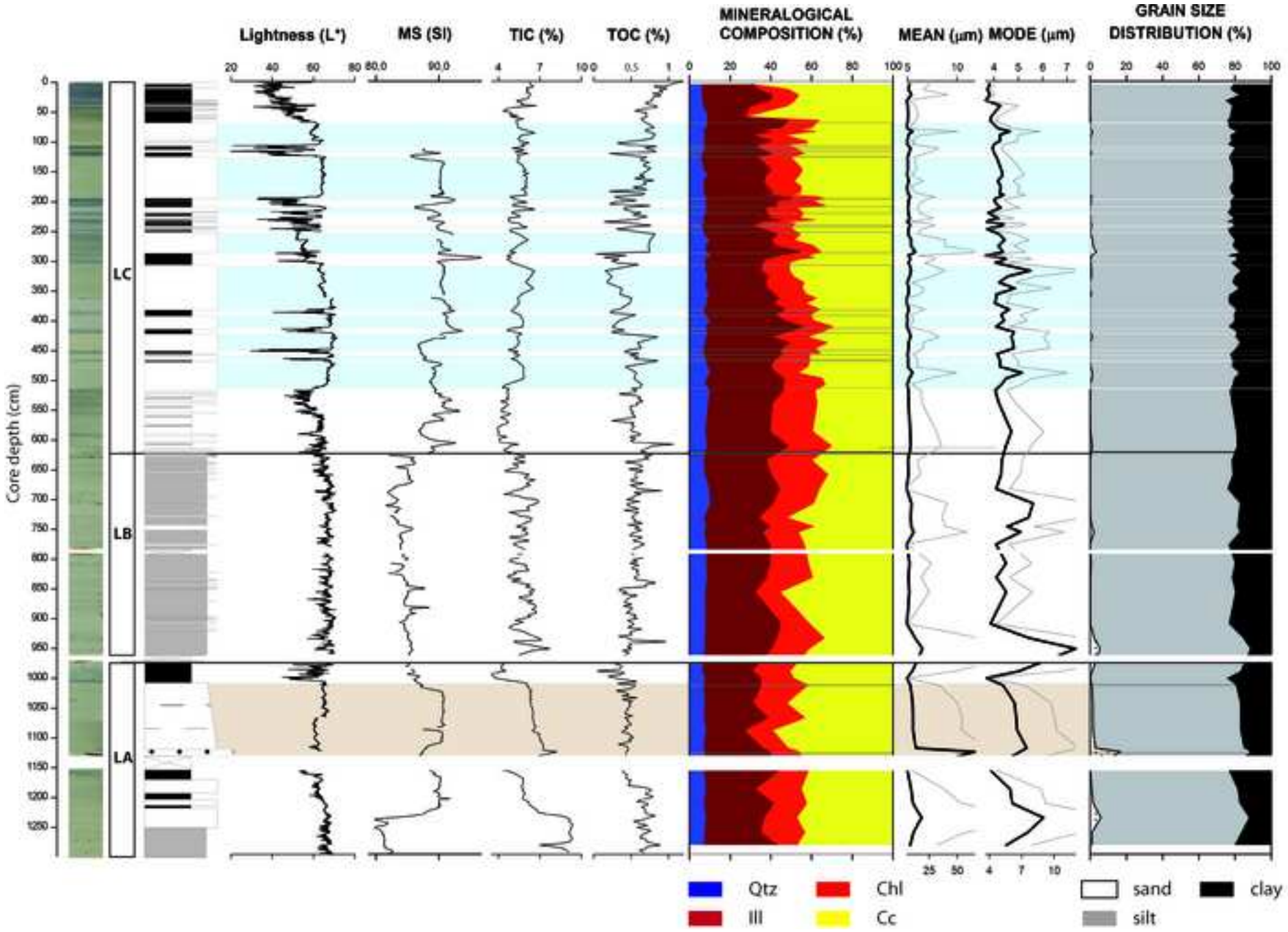

Figure 4

Click here to download high resolution image

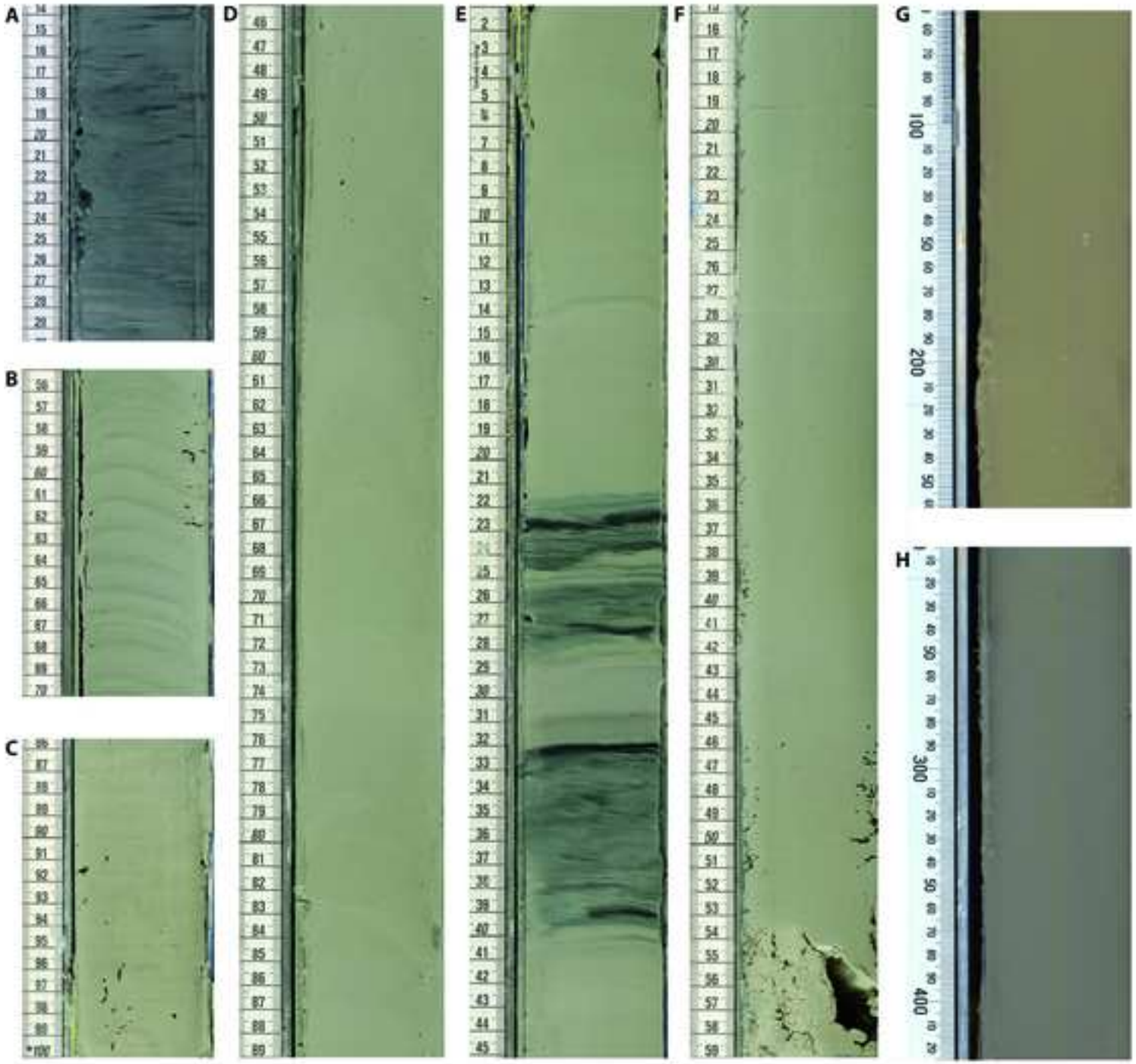

Figure 5

Click here to download high resolution image

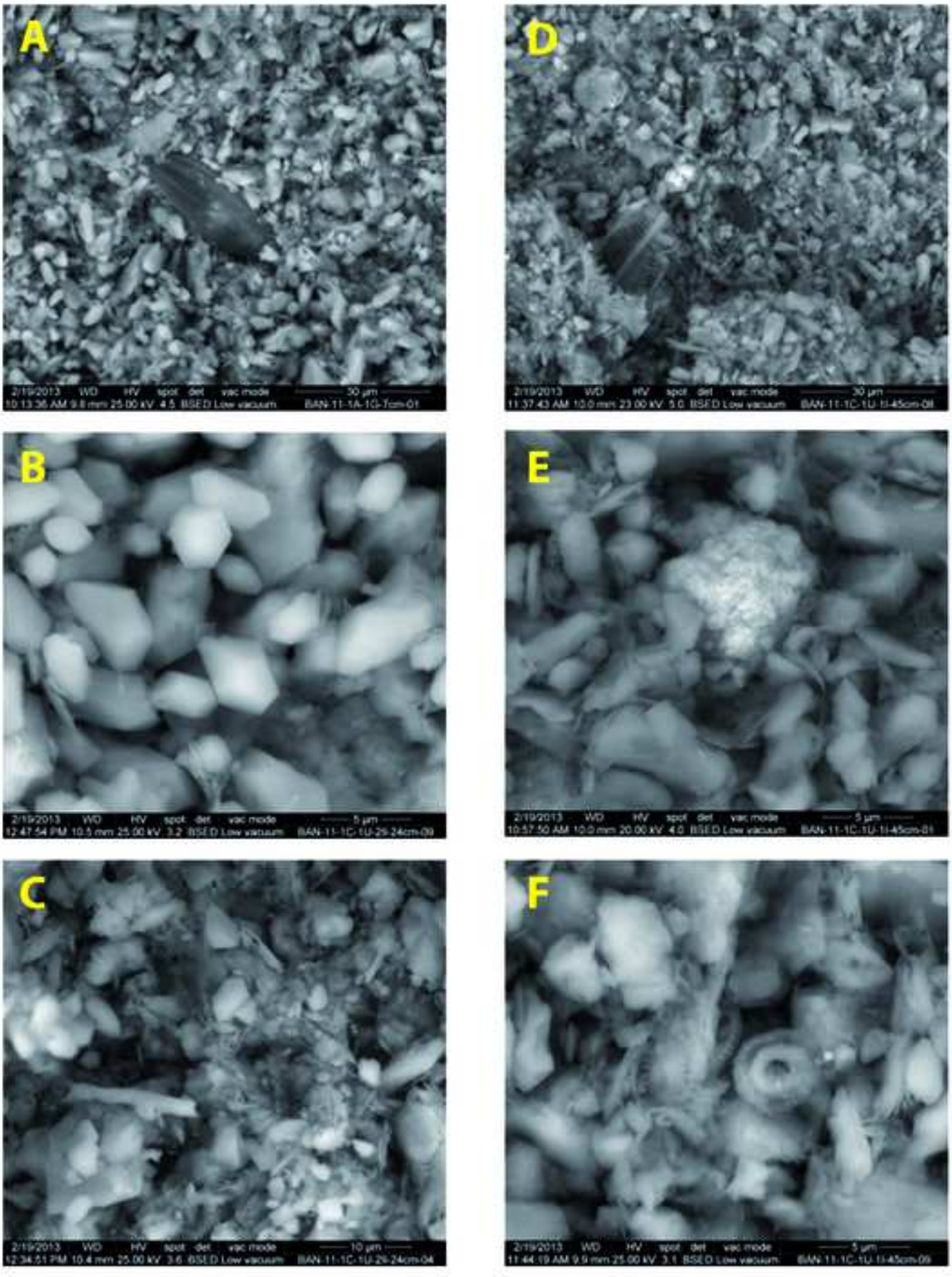

Figure 6

Click here to download high resolution image

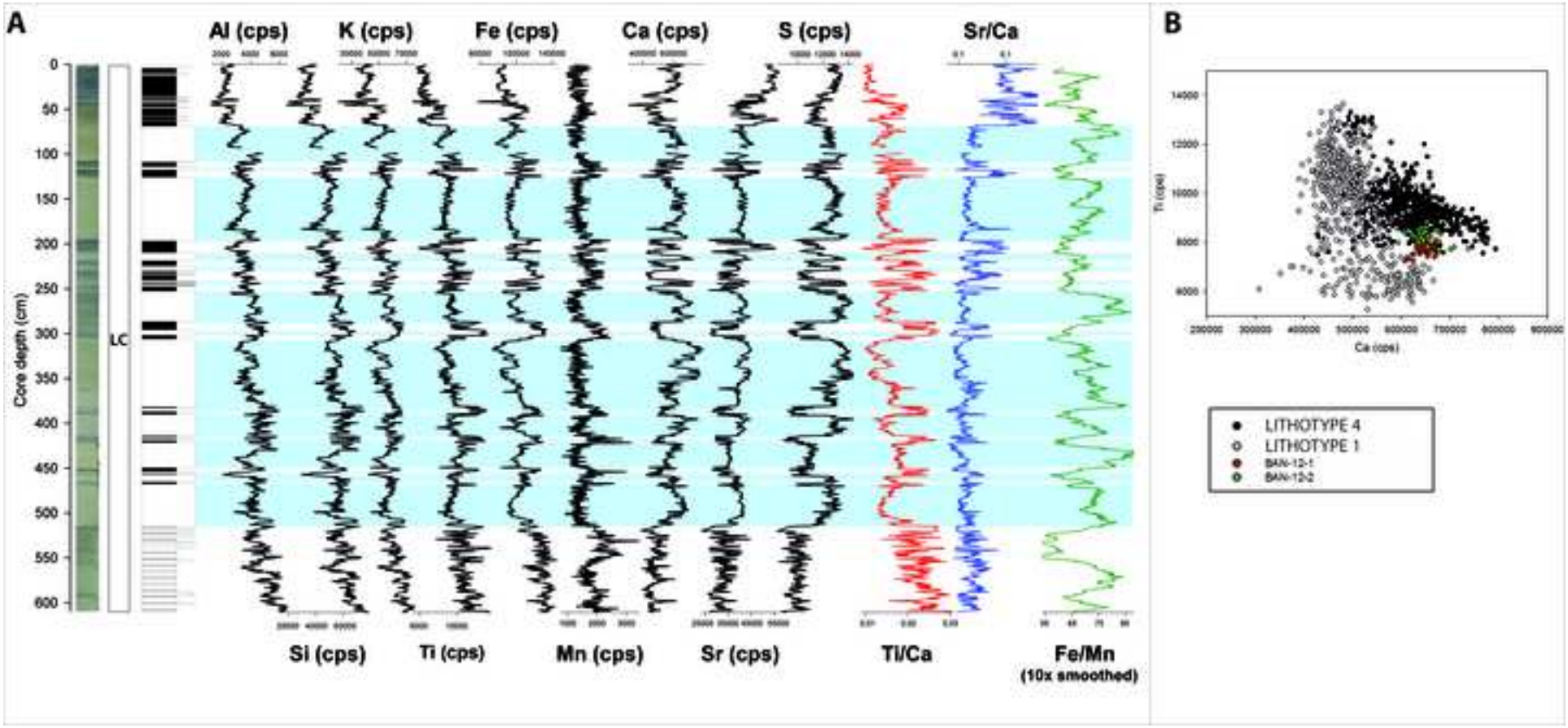

Figure 7

Click here to download high resolution image

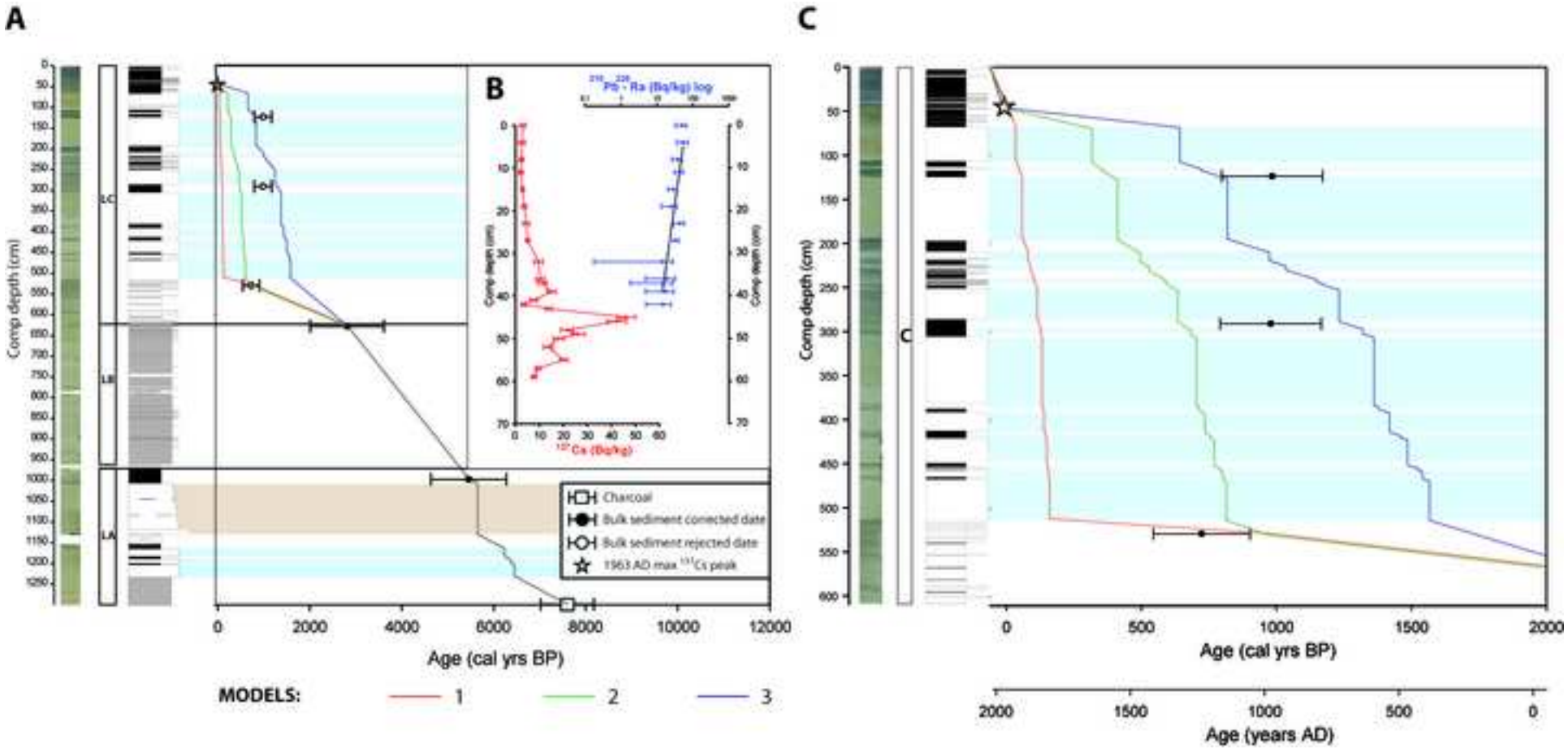

Figure 8

Click here to download high resolution image

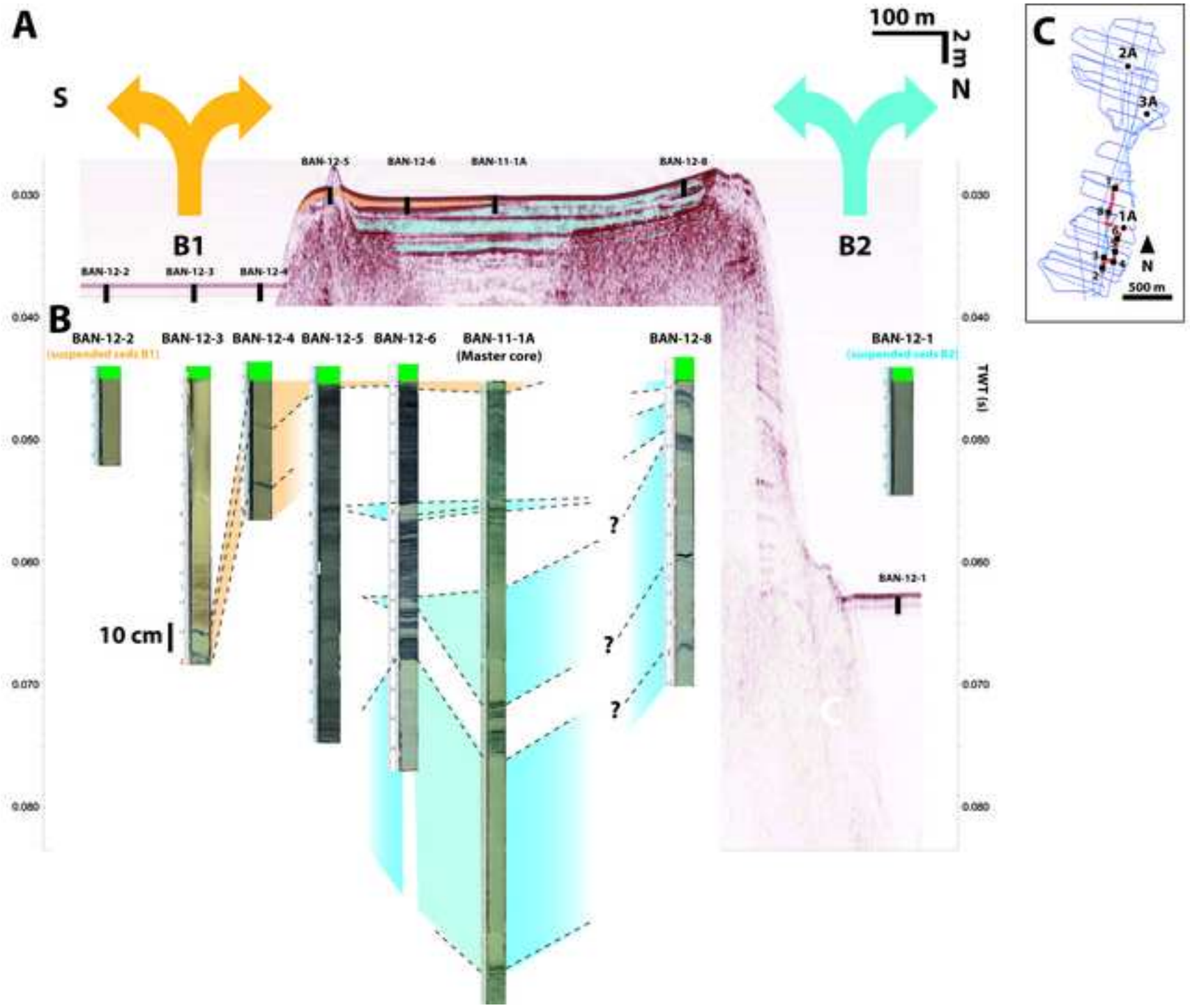

Table 1

Click here to download Table: table 1.docx

Lithotype		*Sedimentological features*	*Compositional parameters*	*Depositional subenvironment/ process*
Banded and laminated	**1**	***Dark-grey to black, massive to banded, carbonate-rich silts with diatoms*** Fine grained carbonate mud composed by up to 10 µm hexagonal calcite grains with abundant to frequent ca. 50-60 µm reworked occasional reworked littoral carbonate-rich particles (ostracods, charophytes and carbonate coatings). Frequent ca. 25 µm detrital carbonate particles, plant remains and diatoms, locally abundant. Occasional quartz grains and < 20µm pyrite framboids.	**TIC** = 3.3% - 6.7 % **TOC** = 0.0% - 1.2 % **Mean GS** = 5 – 18 µm **Mineralogy**: **Cc**= 42.3%, **Ill** = 32.5%, **Chl**= 17.7%, **Qtz**= 7.4%	Deep, monomictic, occasionally anoxic brackish to freshwater lake with permanent, low-concentration turbidity plumes
	2	***Laminated fcs comprising alternating mm to 1 cm thick black and light-grey fine-grained silts*** Black laminae: Fine-grained (up to 10 µm) hexagonal to sub-hexagonal calcite grains with abundant diatoms, up to 100 µm reworked littoral carbonate particles and frequent 20-30 µm detrital grains of quartz and carbonates. Light grey laminae: fine-grained, up to 10 µm irregular, reworked calcite crystals with frequent up to 40 µm clastic quartz and non-biogenic carbonates. Occasional to frequent up to 50 µm reworked littoral carbonate-rich particles.	**TIC** = 3.9 % – 6.2 % **TOC** = 0.2 %- 1.1 % **Mean GS** = 6.0 – 8.4 µm **Mineralogy: Cc** = 39.5%, **Ill** = 32.7%, **Chl** = 19.5%, **Qtz** = 8.2%	Relatively deep, carbonate-producing lake with seasonal anoxic hypolimnetic conditions
	3	***Grey, barely laminated to massive, carbonate-rich silts with evidences of bioturbation*** 30-50 µm reworked biogenic carbonate particles with abundant up to 50 µm irregularly shaped detrital grains of quartz and carbonates. Frequent fine-grained, up to 10 µm calcitic mud.	**TIC** = 4.4% – 9.3% **TOC** = 0.3%- 1.0 % **Mean GS** =4.8 – 18.9 µm **Mineralogy: Cc** = 51.6%, **Ill** = 26.5%, **Chl** = 15.1%, **Qtz** = 6.9%	Shallow, carbonate-producing brackish lake with oxic conditions
Massive	**4**	***Light grey, massive fine-grained, carbonate-rich silts, occurring as mm to cm-thick intercalations or cm to dm-thick homogeneous layers*** Up to 10 µm fine-grained irregularly-shaped calcite mud with abundant reworked diatoms. Frequent up to 50 µm reworked carbonate particles, sub-circular calcareous algae and pyrite framboids. Occasional plant remains.	**TIC** = 4.3% -6.8 % **TOC** = 0.1% - 0.9 % **Mean GS** = 5 – 12.6 µm **Mineralogy: Cc** = 44.7%, **Ill** = 31.7%, **Chl** = 16.2%, **Qtz** = 7.4%	Fluidization events and associated periodical and intense turbidity plumes

5	***Light grey/yellowish, massive, fine-grained, up to 1 m thick fining upwards sequences ranging from coarse to fine-grained silts*** Dominant 10-15 µm reworked, sub-rounded to hexagonal calcite grains with reworked littoral carbonate-rich particles (up to 50-60 µm), more frequent towards the base.	**TIC** = 4.5 % - 7.3% **TOC** = 0.3 % - 0.6 % **Mean GS** = 8.2 – 13.0 µm **Mineralogy: Cc** = 40.9%, **Ill** = 32.7%, **Chl** = 18.8%, **Qtz** = 7.7%	Mass-wasting processes
6	***Light grey/yellowish, massive, fine-grained, carbonate-rich sands*** 100-300 µm sub-rounded, biogenic, reworked carbonate particles with abundant up to 100 µm coarse, high relief detrital grains of quartz and non-biogenic carbonates. Abundant fine-grained matrix composed of up to 10 µm sub-rounded calcite crystals.	**TIC** = 7.2% - 8.8% **TOC** = 0.4% - 0.5 % **Mean GS** = 65.5 µm **Mineralogy: Cc** = 57.9%, **Chl** = 18.1%, **Ill** = 15.4%, **Qtz** = 8.6%	Mass-wasting processes

Table 1. Lithotypes defined for the Lake Banyoles sequence, including sedimentological features, main compositional parameters (TIC = Total Inorganic Carbon, TOC = Total Organic Carbon, GS = Grain Size and mineralogical content (%), including: quartz (Qtz), chlorite (Chl), illite (Ill) and calcite (Cc)) and depositional subenvironments and/or process interpreted for each case

Comp depth (cm)	*Unit*	*Laboratory code*	*Type of material*	*AMS ^{14}C age (yr B.P.)*	*Corrected AMS ^{14}C age*	*Calibrated corrected age (cal yrs BP) (2σ range)*
44,5	LC	D-AMS 001611	Bulk organic matter	5460 ± 35	-13 ± 35	*Modern*
123	LC	D-AMS 001114	Bulk organic matter	6537 ± 36	1064 ± 71	984 ± 187
197,7	LC	D-AMS 001113	Bulk organic matter	5441 ± 33	-32 ± 68	*Modern*
290,5	LC	D-AMS 001609	Bulk organic matter	6519 ± 31	1046 ± 66	979 ± 187
528,8	LC	D-AMS 001112	Bulk organic matter	6217 ± 52	744 ± 87	723 ± 179
627,2	LB	D-AMS 001111	Bulk organic matter	5743 ± 39	2718 ± 324	2808 ± 802
996,1	LA	D-AMS 001610	Bulk organic matter	7813 ± 40	4788 ± 325	5453 ± 824
1297,9	LA	D-AMS 001110	Bulk organic matter	9790 ± 54	6765 ± 339	7600 ± 580
1297,9	LA	ETH-45854	Charcoal	6765 ± 285	6765 ± 285	7600 ± 580

Table 2. Radiocarbon dates used for the construction of the age model for the Lake Banyoles sequence. A correction of 3025 ± 35 ^{14}C years was applied to bulk sediment samples from units LA and LB, and 5473 ± 285 ^{14}C years to uppermost lithological unit LC. Corrected dates were calibrated using CALIB 6.0 software and the INTCAL09 curve (Reimer et al., 2009); and the mid-point of 95.4% (2σ probability interval) was selected.